One-Step Generative Policies with Q-Learning: A Reformulation of MeanFlow

Zeyuan Wang ¹, Da Li ^{2,3}, Yulin Chen ¹, Ye Shi ⁴, Liang Bai ¹, Tianyuan Yu ¹ *, Yanwei Fu ^{5,6},

¹Laboratory for Big Data and Decision, National University of Defense Technology, China
 ² Samsung AI Center Cambridge ³ Queen Mary University of London ⁴ ShanghaiTech University
 ⁵ Fudan University ⁶ Shanghai Innovation Institute

{wzeyuan,ty.yu}@nudt.edu.cn, dali.academic@gmail.com, shiye@shanghaitech.edu.cn, yanweifu@fudan.edu.cn

Abstract

We introduce a one-step generative policy for offline reinforcement learning that maps noise directly to actions via a residual reformulation of MeanFlow, making it compatible with Q-learning. While one-step Gaussian policies enable fast inference, they struggle to capture complex, multimodal action distributions. Existing flow-based methods improve expressivity but typically rely on distillation and two-stage training when trained with Q-learning. To overcome these limitations, we propose to reformulate MeanFlow to enable direct noise-to-action generation by integrating the velocity field and noise-to-action transformation into a single policy network—eliminating the need for separate velocity estimation. We explore several reformulation variants and identify an effective residual formulation that supports expressive and stable policy learning. Our method offers three key advantages: 1) efficient one-step noise-to-action generation, 2) expressive modelling of multimodal action distributions, and 3) efficient and stable policy learning via O-learning in a single-stage training setup. Extensive experiments on 73 tasks across the OG-Bench and D4RL benchmarks demonstrate that our method achieves strong performance in both offline and offline-toonline reinforcement learning settings. Code is available at https://github.com/HiccupRL/MeanFlowQL.

Introduction

Offline reinforcement learning (RL) enables the training of decision-making agents from fixed datasets, eliminating the need for online environment interaction (Hafner and Riedmiller 2011). This is especially valuable in safety-critical domains such as robotics, autonomous driving, and healthcare, where exploration can be costly or risky. A central challenge in offline RL is learning *expressive yet efficient policies* that can capture complex, multi-modal action distributions while remaining amenable to stable value-based optimisation.

One-step Gaussian policies are widely adopted due to their fast and simple sampling procedures. However, their uni-modal nature limits expressivity, especially in tasks that involve diverse or multi-modal behaviour patterns (Pomerleau 1988; Tarasov et al. 2023a). In contrast, flow- and diffusion-based generative models (Esser et al. 2024; Jin et al. 2025;

Copyright © 2026, Association for the Advancement of Artificial Intelligence (www.aaai.org). All rights reserved.

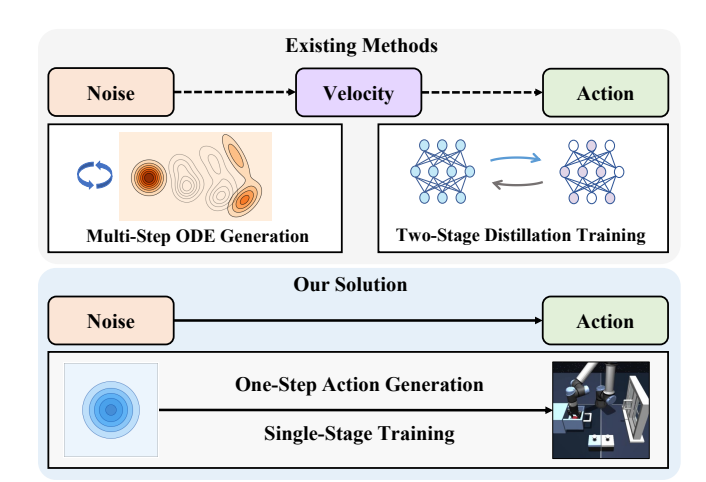


Figure 1: Existing generative policy approaches v.s. our proposed solution. Existing methods rely on velocity-based modelling, requiring either multi-step ODE integration or two-stage distillation training. In contrast, our method enables one-step action generation directly from noise, trained via a single-stage, end-to-end process—improving both inference efficiency and training stability.

Liu et al. 2024) have shown strong potential for modelling rich, multimodal distributions and have been increasingly applied in offline RL (Park, Li, and Levine 2025; Mees et al. 2024; O'Neill et al. 2024). Most of these approaches, however, focus on *behaviour cloning* (Pomerleau 1988; Chi et al. 2023; Prasad et al. 2024; Zhang et al. 2025; Sheng et al. 2025) and do not support *value-based learning*, limiting their ability to improve policies with Q-functions.

Integrating expressively generative models into Q-learning is challenging. Flow- and diffusion-based policies typically require *multi-step generation*, relying on ODE or SDE solvers, which introduce *backpropagation through time (BPTT)* (Ding and Jin 2024). This leads to computational inefficiencies and instability when optimizing jointly with a critic. To address this, recent works (Chen, Wang, and Zhou 2024; Park, Li, and Levine 2025) adopt a *two-stage distillation framework*, where a multi-step generative policy is first trained via behaviour cloning, then distilled into a one-step policy together optimised with Q-values. While this avoids BPTT, it introduces additional complexity and degrades the

^{*}Corresponding author

final policy's expressivity due to the distillation bottleneck.

In this work, we propose an *expressive one-step generative policy* that can be directly optimized with Q-functions in a *single-stage* training process—without requiring distillation or iterative sampling. Our approach is inspired by the MeanFlow framework (Geng et al. 2025), which enables efficient one-step sampling by modelling the average velocity of noise-to-data transitions. Although MeanFlow was originally developed for visual generation, we repurpose its structure for learning a generative policy in offline RL.

A direct adaptation of MeanFlow involves two separate processes: first, predicting a velocity vector, and then integrating it to transform noise into actions. However, we find that this approach leads to a critical issue in Q-learning: during early training, the generated actions frequently lie outside valid bounds and require *post-hoc clipping*. This mismatch between policy outputs and the actions used for Bellman target computation destabilizes training and degrades performance.

One might attempt to simplify MeanFlow by reformulating its two-step process into a single network with direct, residual mapping—i.e., using $a=\epsilon-u(\epsilon,b,t)$, where a is predicted action, $\epsilon \sim \mathcal{N}(0,I)$ is sampled noise, u is a learnable average velocity field, and b,t denote the start and end times. While this formulation eliminates the need for explicit velocity integration, we find that such a naive reformulation suffers from poor training dynamics. In toy experiments, this model underfits and fails to capture multimodal data distributions, reintroducing the risk of generating mismatched actions—mirroring the challenges seen in the original two-step MeanFlow adaptation.

To address these issues, we propose a revised *residual MeanFlow formulation* with a carefully constructed mapping:

$$g(a_t, b, t) = a_t - u(a_t, b, t),$$
 (1)

where a_t is a linear interpolation between an offline-dataset action and noise. Unlike the naive form, this formulation retains theoretical equivalence to the original MeanFlow under mild assumptions, with guarantees provided by the *Universal Approximation Theorem* (Tabuada and Gharesifard 2021) (see Methodology and Appendix B.3 for further discussion).

Our method offers three key advantages: i) Efficient one-step noise-to-action generation without iterative inference; ii) Expressive modelling of complex, multimodal action distributions via reformulated MeanFlow-based policies; iii) Stable joint optimisation with Q-functions through direct, single-stage training—without distillation. In addition, we introduce two practical enhancements to improve the efficacy of our method, including a value-guided rejection sampling and an adaptive behaviour cloning regularisation (See Methodology section for details). Collectively, they contribute to the robustness and performance of our one-step policy, leading to strong results across 73 tasks on the OGBench (Park et al. 2025) and D4RL (Fu et al. 2020) benchmarks in both the offline and offline-to-online settings (see Experiments).

Preliminary

Offline Reinforcement Learning

In this work, we consider a Markov Decision Process (MDP) $\mathcal{M} = (\mathcal{S}, \mathcal{A}, r, \rho, p, \gamma)$ (Sutton, Barto et al. 1998; Puterman

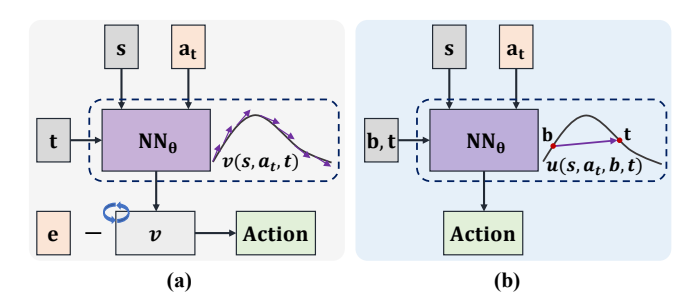


Figure 2: Comparison between traditional and proposed flow-based policy network schemes. (a) Given state s and noisy input a_t , traditional flow-based methods estimate the *instantaneous velocity* $v(s, a_t, t)$ at time t, as a one-step approximation of multi-step ODE integration. (b) Our method reformulate MeanFlow to estimate the *average velocity* over the interval [b, t], enabling direct one-step action generation.

2014), where $\mathcal S$ denotes the state space, $\mathcal A\subseteq\mathbb R^d$ is the d-dimensional continuous action space, $r:\mathcal S\times\mathcal A\to\mathbb R$ is the reward function, $\rho\in\Delta(\mathcal S)$ is the initial state distribution, p(s'|s,a) defines the transition dynamics, and $\gamma\in[0,1)$ is the discount factor. In offline RL, the agent does not interact with the environment during training. Instead, it learns from a fixed dataset $\mathcal D=\{\tau^{(n)}\}_{n=1}^N$ composed of trajectories $\tau=(s_0,a_0,r_0,\ldots,s_H,a_H,r_H)$, collected by some unknown behaviour policy. The typical objective is to learn a policy $\pi_\theta(a|s)$ that maximizes the expected discounted return with some regularization:

$$\mathcal{L}_{\pi}(\theta) = -J(\pi_{\theta}) + \alpha R(\pi_{\theta}), \tag{2}$$

where $J(\pi_{\theta}) = \mathbb{E}_{\tau \sim p^{\pi_{\theta}}(\tau)} \left[\sum_{t=0}^{H} \gamma^{t} r(s_{t}, a_{t}) \right], p^{\pi_{\theta}}(\tau)$ is the trajectory distribution induced by π_{θ} under the dynamics p and initial state ρ , and α controls the regularisation strength.

In the behaviour cloning (BC) regularised actor-critic learning framework, the objective in Eq 2 becomes

$$\mathcal{L}_{\pi}(\theta) = \mathbb{E}_{s, a \sim \mathcal{D}, a^{\pi} \sim \pi_{\theta}} \left[-Q_{\phi}(s, a^{\pi}) - \alpha \log \pi_{\theta}(a|s) \right],$$

where the second term is a behaviour cloning regularizer, \mathcal{D} denotes the offline dataset and $Q_{\phi}(s,a)$ is the critic parameterised by ϕ , which is trained to minimise the Bellman error as follows

$$\mathcal{L}_{Q} = \mathbb{E}_{(s,a,r,s') \sim \mathcal{D}} \left[Q_{\phi}(s,a) - (r + \gamma Q_{\bar{\phi}}(s', \pi_{\theta}(s'))) \right]^{2}, \tag{4}$$

where $\bar{\phi}$ corresponds to the target network.

Flow Matching and MeanFlow

Flow Matching learns to transform noise into data via timedependent velocities, whereas MeanFlow enables one-step sampling by modelling the time-averaged velocity.

Flow matching. Flow matching (Lipman et al. 2023; Liu, Gong, and Liu 2023) is a generative modelling framework that learns a continuous time-dependent velocity field bridging a simple base distribution and a complex data distribution. In our context, let $e \sim p_{\rm prior}$ be sampled from a simple

prior (e.g. a standard Gaussian) and $a \sim p_{\text{data}}$ from the empirical action data distribution. We consider an interpolation $a_t = (1-t) \, a + t \, e$ for $t \in [0,1]$. Flow matching trains a velocity field $v_{\theta}(a_t,t)$ to predict the ground-truth displacement between a and e. Specifically, one trains v_{θ} by minimizing:

where $a_t = (1 - t)a + te$ as above. By learning to predict e - a, the model captures the time-dependent instantaneous velocity needed to transform a into e (or vice versa).

MeanFlow. MeanFlow (Geng et al. 2025) builds on flow matching by introducing an *average velocity* field $u(a_t,b,t)$. For any $0 \le b < t \le 1$, the average velocity is defined as the time-average of the instantaneous velocity v over the interval [b,t]:

$$u(a_t, b, t) := \frac{1}{t - b} \int_b^t v(a_\tau, \tau) d\tau. \tag{6}$$

Differentiating both sides with respect to t (treating b as constant) yields the *MeanFlow Identity* as introduced in (Geng et al. 2025):

$$u(a_t, b, t) = v(a_t, t) - (t - b) \frac{\partial}{\partial t} u(a_t, b, t).$$
 (7)

MeanFlow establishes a principled relationship between the average velocity u and the instantaneous velocity v. Crucially, it enables *one-step* generation: by choosing b=0 and t=1 in (6), one can generate a sample in a single step:

$$\hat{a} = e - u_{\theta}(e, b = 0, t = 1),$$
 (8)

where $e \sim \mathcal{N}(0, I)$ and u_{θ} is the learned average velocity function. This formula generates \hat{a} via one-step velocity estimation using the learned u_{θ} , without integrating over time.

Flow policies in RL. Recent works have proposed using flow matching to learn policies in RL. In such flow policies, the policy π_{θ} is implicitly defined by a state-conditional velocity field $v_{\theta}(s, a_t, t)$. For example, one offline training objective for a flow policy is:

$$\mathcal{L}_{\text{Flow}}(\theta) = \underset{\substack{(s,a) \sim D, \\ e \sim \mathcal{N}(0,I), \ t \sim \mathcal{U}(0,1)}}{\mathbb{E}} \left[\| v_{\theta}(s, a_t, t) - (e - a) \|_2^2 \right],^{1}$$

with $a_t = (1 - t)a + te$. The flow model v_θ here plays the role of a generative policy that, given state s and noise e, outputs a velocity which can be used to produce an action.

A straightforward way to integrate flow policies into offline RL is to replace the BC loss in the actor objective (3) with the flow matching loss (9). Compared to Gaussian or diffusion-based policies, flow policies offer a powerful yet efficient framework for modelling multi-modal action distributions.

Methodology

Standard Gaussian policies generate actions directly from noise and offer efficient inference, but they lack the expressivity needed to model complex, multimodal action distributions. Flow-based generative policies improve expressivity through iterative sampling, yet their integration with Q-learning requires backpropagation through time (BPTT), making joint training unstable and inefficient. Distillation-based approaches bypass BPTT by employing a two-stage training process, which sacrifices model expressivity in the final one-step policy.

This raises a key question: Can we design a generative policy that enables one-step action sampling while preserving the expressivity of flow-based models and supporting stable joint training with Q-functions? To answer this question, we introduce our idea of reformulating MeanFlow into an end-to-end policy function.

Naive MeanFlow Policies

A straightforward approach to enable one-step action generation is to directly adopt the original MeanFlow formulation, which estimates the average velocity and uses it to transform noise into actions. Specifically, MeanFlow generates an action as follows:

$$v_{\text{ave}} = u(e, b=0, t=1), //\text{vel. est.}$$

 $\hat{a} = e - v_{\text{ave}}, //\text{vel. integ.}$ (10)

where $e \sim \mathcal{N}(0,I)$ is Gaussian noise, and u denotes the learned average velocity field.

Although this formulation avoids iterative velocity integration over time and thus enables efficient inference, it suffers from a key limitation: the decoupled processes reduce controllability. The sampled noise e often induces the generated actions to fall outside the valid action bounds (e.g., [-1,1]), especially in early training when u is inaccurate. Consequently, the generated actions frequently require post-hoc clipping, which breaks the alignment between the policy output and the actions used in the Bellman target. This mismatch destabilises Q-learning and can degrade overall performance, as shown in the results in Experiments and analysis in the Appendix.

Reformulated MeanFlow: Direct Noise-to-Action Mapping

The core limitation of the original MeanFlow formulation lies in its inference pipeline: noise \rightarrow velocity \rightarrow action. This decoupled design, which first predicts a velocity and then transforms noise into an action, often leads to instability—particularly during early training when the estimated velocity field is still inaccurate.

A natural workaround is to reformulate MeanFlow into a single-step residual form, such as $a=\epsilon-u(\epsilon,b,t)$, effectively merging velocity estimation and action generation into one forward pass. However, this naive reformulation performs poorly in practice: it fails to capture multimodal distributions, as shown in the toy experiments in the Appendix.

We propose a revised *residual MeanFlow formulation* with a carefully constructed mapping

$$g(a_t, b, t) = a_t - u(a_t, b, t),$$
 (11)

¹Note that *state* s is an important input of our model. But for simplicity, and to save space in our equations, we will continue to denote the pair (s, a_t) simply by a_t

which reduces to the original MeanFlow output when b=0, t=1, and $a_1=e$:

$$g(e, b = 0, t = 1) = e - u(e, b = 0, t = 1).$$
 (12)

This revised residual transformation satisfies two key desiderata: 1) The mapping g_{θ} retains the representational capacity of the original MeanFlow velocity function u_{θ} , as guaranteed by the *Universal Approximation Theorem* (*UAT*) (Leshno et al. 1993; Tabuada and Gharesifard 2021). 2) For inputs of the form given in Equation 10, the model enables well-bounded one-step outputs (typically within the [-1,1] range) even in the early stages of training through appropriate initialisation strategies, such as zero initialisation or small-variance Kaiming initialisation. A more detailed derivation of this formulation is provided in Appendix B.

This proposed formulation enables the network to learn a complete noise-to-action transformation directly, without depending on intermediate velocity estimation. Our method alleviates the early-stage instability caused by post-hoc clipping, while preserving the expressivity and efficiency inherent in the MeanFlow framework.

Training Objective of Our One-Step Policy

To train our residual mapping $g_{\theta}(a_t, b, t)$, we leverage the *MeanFlow Identity*, which defines the average velocity field $u(a_t, b, t)$ as the difference between the instantaneous velocity $v(a_t, t)$ and its time derivative $\frac{d}{dt}u(z_t, b, t)$, as shown in Eq 7. Specifically, we follow (Geng et al. 2025) to optimise g_{θ} to satisfy this identity by minimising the following objective:

$$\mathcal{L}_{\mathrm{MFI}}(\theta) = \mathbb{E} \left\| g_{\theta}(a_t, b, t) - \mathrm{sg}(g_{\mathrm{tgt}}) \right\|_2^2, \tag{13}$$

where \mathcal{L}_{MFI} represents loss of MeanFlow Identity, $sg(\cdot)$ denotes the stop-gradient operation. The core challenge lies in constructing an accurate regression target g_{tgt} , which we derive as follows.

Recall from our reformulation that:

$$g(a_t, b, t) = a_t - u(a_t, b, t).$$
 (14)

We substitute $u(a_t, b, t)$ using the velocity-based formulation from the MeanFlow Identity in Eq 7 which leads to:

$$g(a_t, b, t) = a_t - [v(a_t, t) - (t - b)\frac{d}{dt}(a_t - g(a_t, b, t))]$$

$$= a_t - [v(a_t, t) - (t - b)(v(a_t, t) - \frac{d}{dt}g(a_t, b, t))]. \tag{15}$$

To compute the total time derivative $\frac{d}{dt}g(a_t, b, t)$, we apply the chain rule:

$$\frac{d}{dt}g(a_t, b, t) = \frac{da_t}{dt} \cdot \partial_{a_t}g + \frac{db}{dt} \cdot \partial_b g + \frac{dt}{dt} \cdot \partial_t g. \quad (16)$$

Since $\frac{da_t}{dt}=v(a_t,t),\, \frac{db}{dt}=0,$ and $\frac{dt}{dt}=1,$ we simplify to:

$$\frac{d}{dt}g(a_t, b, t) = v(a_t, t) \cdot \partial_{a_t}g + \partial_t g. \tag{17}$$

Substituting Equation 17 back into Equation 15, finally get:

$$g_{tgt} = a_t + (t - b - 1) \cdot v(a_t, t) - (t - b) \cdot [v(a_t, t) \cdot \partial_{a_t} g + \partial_t g].$$
(18)

Algorithm 1 One-Step Generative Policy with Q-learning

```
while not converged do
      Sample batch \{(s, a, r, s')\} \sim \mathbb{D}
      \triangleright Train Critic Q_{\phi}
      e \sim \mathbb{N}(0, I_d)
      \{a_1, \dots, a_K\} = \operatorname{vmap}(g_\theta)(s, e_{1:K}, b = 0, t = 1)
      a' \leftarrow \arg \max_{a_i} Q(s, a_i), \quad a_i \in \{a_1, \dots, a_K\}
      Update \phi to minimize \mathbb{E}[(Q_{\phi}(s, a) - r - \gamma Q_{\bar{\phi}}(s', a'))^2]
      \triangleright Train One-Step MeanFlow Policy \pi_{\theta}
      t, b \sim \mathbb{U}(0, 1)
      a_t = (1 - t)a + te
      v = e - a
     \begin{split} g, dgdt &= \mathtt{jvp}(g_\theta, (s, a_t, b, t), (s, v, 0, 1)) \\ g_{\mathtt{tgt}} &= a_t + (t - b - 1)v - (t - b)dgdt \\ err &= g - [g_{\mathtt{tgt}}]_{\mathtt{sg}} \end{split}
      \mathcal{L}_{MFI} = metric(err)
                                                     a^{\pi} \leftarrow g_{\theta}(s, e)
      \mathcal{L}_Q = -Q_\phi(s, a^\pi)
                                                                         Update \theta to minimize \mathcal{L}_Q + \alpha \mathcal{L}_{MFI}
return One-step policy g_{\theta}
```

$$\begin{array}{ll} \textbf{function Policy}(s) & \rhd \text{ One-Step Policy} \\ & \{a_1,\ldots,a_K\} = \mathsf{vmap}(g_\theta)(s,e_{1:K},b=0,t=1) \\ & a' = \arg\max_{a_i}Q(s,a_i), \quad a_i \in \{a_1,\ldots,a_K\} \\ & \textbf{return } a' \end{array}$$

It is worth noting that the formulation remains agnostic of any network parameterisation. The target relies solely on the instantaneous velocity v and the noisy data a_t as ground-truth signals, without requiring any integral computation. Specifically, recall that $a_t = (1-t)a+te$; by default, the instantaneous velocity $v(a_t,t)$ simplifies to e-a. The gradient terms $\partial_{a_t}g$ and ∂_tg are readily computed using the current policy network g_θ . Full algorithmic details are provided in Algorithm 1.

Value-Guided Action Selection in Bellman Iteration

While performing behaviour cloning, we also need to update the critic function through the Bellman equation iteratively. However, despite the efficiency gains brought by our one-step generative policy, its stochastic sampling of the input noise induces some action-sampling variance, which destabilises Bellman updates and may lead to divergence during critic training. To address this issue, we adopt a value-guided rejection sampling scheme for action selection.

Furthermore, by utilising the vmap function in the JAX framework, we can sample these candidates in parallel and evaluate them with negligible computational overhead. Formally, we define the value-guided behaviour policy sampling as

$$\pi_{\theta}^{K}(a|s) \triangleq \underset{a \in \{a_{1}, \dots, a_{K} \sim g_{\theta}(s, e, b = 0, t = 1)\}}{\operatorname{argmax}} Q(s, a),$$

where K actions are sampled simultaneously from the learned policy. The action with the highest Q-value is selected for the Bellman iteration as follows:

$$\mathcal{L}_{Q} = \mathbb{E}_{(s,a,r,s') \sim \mathcal{D}} \Big[\big(Q_{\phi}(s,a) - \big(r + \gamma \, Q_{\bar{\phi}}(x',a') \big) \big)^{2} \Big],$$
(19)

where $a' \sim \pi_{\theta}^K(a|s')$, $\bar{\phi}$ denotes a delayed target network to promote training stability. We incorporate value-guided action sampling into the Bellman update without modifying the underlying policy model, effectively filtering out low-quality samples and focusing optimisation on more promising regions of the action space. Consequently, it enhances both training stability and final policy performance.

Adaptive Behaviour-Cloning Coefficient

Overall, the training objective for our one-step generative policy with Q-learning can be formalised as follows:

$$\theta^{\star} = \arg\max_{\theta} \mathbb{E}_{\substack{(s,a) \sim \mathcal{D} \\ a^{\pi} \sim \pi_{\theta}(\cdot \mid s)}} \left[\underbrace{Q_{\phi}(s, a^{\pi})}_{\text{Q loss}} - \underbrace{\alpha \mathcal{L}_{\text{MFI}}}_{\text{BC loss}} \right]. (20)$$

Empirically, the choice of α is crucial, as it directly governs the trade-off between behaviour cloning and Q-learning. To adaptively balance their contributions, we dynamically adjust the behaviour cloning coefficient α according to historic training dynamics. Concretely, we maintain a moving average $\overline{\mathcal{L}_Q}$ of the behaviour cloning loss over a sliding window and update α as follows:

$$\alpha \leftarrow \begin{cases} 1.2 \times \alpha, & \text{if } \mathcal{L}_Q > 5 \cdot \overline{\mathcal{L}_Q}, \\ 0.8 \times \alpha, & \text{if } \mathcal{L}_Q < 0.2 \cdot \overline{\mathcal{L}_Q}, \\ \alpha, & \text{otherwise.} \end{cases}$$
 (21)

Despite differences, this strategy is inspired by the adaptive KL penalty introduced in PPO (Schulman et al. 2017) and ensures that the behaviour cloning regularisation remains neither dominant nor negligible during training. Thus, this stabilises training and results in more balanced policy updates. Empirical evaluations decided the introduced scaling factors.

Experiments

In this section, we present experimental evaluations of our one-step generative policy with Q-learning, comparing its performance against 10 baselines across 73 tasks. Additionally, we conduct analytical studies to help understand our method.

Experimental Setup

Benchmarks. We evaluate our method on a diverse set of offline RL tasks spanning locomotion and manipulation domains. The primary benchmark is the OGBench suite (Park, Li, and Levine 2025), which includes 50 state-based tasks and 5 visual-based tasks across 10 environments: antmaze-large, antmaze-giant, humanoidmaze-medium, humanoidmaze-large, antsoccer-arena, cube-single, cube-double, scene-play, puzzle-3×3, and puzzle-4×4. Additionally, we include 18 challenging tasks from the D4RL benchmark (Fu et al. 2020), covering antmaze and adroit manipulation scenarios. OGBench tasks feature semi-sparse rewards and complex behavioural distributions, while D4RL tasks are known for their high-dimensional action spaces.

Baselines. We compare our method against ten representative baselines spanning three policy classes. *Gaussian policies* include behavioural Cloning (BC) (Pomerleau 1988), Implicit Q-Learning (IQL) (Kostrikov, Nair, and Levine 2021),

and ReBRAC (Tarasov et al. 2023a). *Diffusion-based policies* include IDQL (Hansen-Estruch et al. 2023), SRPO (Chen et al. 2023a), and Consistency Actor-Critic (CAC) (Ding and Jin 2024). *Flow-based policies* include FAWAC (Nair et al. 2020), FBRAC (Zhang, Zhang, and Gu 2025), IFQL (Wang, Hunt, and Zhou 2022), and Flow Q-Learning (FQL) (Park, Li, and Levine 2025). *Specifically designed for online RL* include Cal-QL (Nakamoto et al. 2023) and PLPD (Ball et al. 2023).

Evaluation metrics. For offline RL, we assess the performance of the methods after a fixed number of gradient steps. Specifically, following (Tarasov et al. 2023b) we avoid reporting the best performance across different evaluation epochs to prevent potential bias in the results. In our experiments, we employ 8 random seeds for state-based tasks and 4 seeds for pixel-based tasks. For the OGBench locomotion and manipulation tasks, performance is measured as the percentage of episodes that achieve the goal. For the D4RL Adroit tasks, we measure binary task success rates (in percentage) for antmaze and normalized returns for adroit, following the original evaluation scheme (Fu et al. 2020). We refer to Appendix D for the full training and evaluation details.

Comparisons with SOTA

Offline RL performance. Following FQL (Park, Li, and Levine 2025), we evaluate our method on the offline subset of the OGBench and D4RL benchmarks, which include diverse tasks with varying dynamics and action dimensionalities. Table 1 shows that our approach achieves strong performance across a wide range of tasks, particularly in environments such as OGBench antmaze, humanoidmaze, puzzle, and visual manipulation, which likely demand expressive and multimodal policy behaviours due to complex dynamics.

Compared to flow-based baselines such as FQL, IFQL, and FBRAC, our method either matches or surpasses their performance while maintaining a simpler one-stage training pipeline and a one-step inference mechanism. Although performance on particularly sparse environments remains modest—such as in giant maze navigation—the results are consistent with broader trends observed across baselines, indicating inherent task difficulty rather than model-specific limitations. (We additionally add an online-finetuning extension on this task as shown in Table 2 and show that although initial offline performance was limited, our method achieved strong improvements after online finetuning, suggesting the bottleneck may lie in the offline dataset.) Overall, the results indicate that our one-step generative policy serves as a viable and competitive approach for offline reinforcement learning.

Offline-to-online transfer. We further evaluate our method in offline-to-online settings following (Park, Li, and Levine 2025) (while adding antmaze-giant-navigate), where policies are first pre-trained on static offline datasets and then fine-tuned through online interaction. As shown in Table 2, our method consistently improves after fine-tuning and achieves strong final performance across a diverse set of tasks. More notably, although the offline performances are not ideal on antmaze-giant-navigate and cube-double-play, our method gains a significant performance boost in the online adaptation.

Table 1: Offline RL results. Our method achieves the best or near-best performance on most of the 73 diverse, challenging benchmark tasks. The performances are averaged over 8 seeds (4 seeds for pixel-based tasks), but the cells without the \pm sign indicate that the numbers are taken from prior works (Tarasov et al. 2023b; Hansen-Estruch et al. 2023; Chen et al. 2023a). See Table 4 in Appendix for the full results.

	Gaus	sian Po	olicies	Diffus	sion Po	licies		Flor	√ Polici	les	
Task Category	BC	IQL	ReBRAC	IDQL	SRPO	CAC	FAWAC	FBRAC	IFQL	FQL	Ours
OGBench antmaze-large-singletask (5 tasks)	11 ±1	53 ±3	81 ±5	21 ±5	11 ±4	33 ±4	6 ±1	60 ±6	28 ±5	79 ±3	81 ±3
OGBench antmaze-giant-singletask (5 tasks)	0 ± 0	4 ± 1	26 ± 8	0 ± 0	0 ± 0	0 ± 0	0 ± 0	4 ± 4	3 ± 2	9 ± 6	0 ± 0
OGBench humanoidmaze-medium-singletask (5 tasks)	2 ± 1	33 ± 2	22 ± 8	1 ± 0	1 ±1	53 ± 8	19 ± 1	38 ± 5	60 ± 14	58 ± 5	$62_{\pm 1}$
OGBench humanoidmaze-large-singletask (5 tasks)	1 ± 0	2 ± 1	2 ± 1	1 ± 0	0 ± 0	0 ± 0	0 ± 0	2 ± 0	11 ± 2	4 ± 2	20 ± 3
OGBench antsoccer-arena-singletask (5 tasks)	1 ± 0	8 ±2	0 ± 0	12 ± 4	1 ± 0	$2_{\pm 4}$	12 ± 0	16 ± 1	33 ± 6	60 ± 2	62 ± 3
OGBench cube-single-singletask (5 tasks)	5 ± 1	83 ± 3	91 ± 2	$95_{\pm 2}$	80 ± 5	85 ± 9	81 ± 4	79 ± 7	$79_{\pm 2}$	96 ± 1	$95_{\pm 2}$
OGBench cube-double-singletask (5 tasks)	2 ± 1	$7_{\pm 1}$	12 ± 1	15 ± 6	2 ± 1	6 ± 2	5 ± 2	15 ±3	14 ± 3	$29_{\pm 2}$	3 ± 2
OGBench scene-singletask (5 tasks)	5 ± 1	28 ± 1	41 ±3	46 ± 3	20 ± 1	40 ± 7	30 ±з	45 ± 5	30 ±з	56 ± 2	60 ± 1
OGBench puzzle-3x3-singletask(5 tasks)	2 ± 0	9 ± 1	21 ± 1	10 ± 2	18 ± 1	19 ± 0	6 ± 2	14 ± 4	19 ± 1	30 ± 1	66 ± 8
OGBench puzzle-4x4-singletask (5 tasks)	0 ± 0	$7_{\pm 1}$	14 ± 1	29 ± 3	10 ± 3	15 ± 3	1 ± 0	13 ± 1	25 ± 5	17 ± 2	$40_{\pm 6}$
D4RL antmaze (6 tasks)	17	57	78	79	74	30 ± 3	44 ± 3	64 ± 7	65 ± 7	84 ± 3	83 ± 2
D4RL adroit (12 tasks)	48	53	59	52 ± 1	51 ± 1	43 ± 2	48 ± 1	50 ± 2	52 ± 1	52 ± 1	54 ± 3
Visual manipulation (5 tasks)	-	$42{\scriptstyle~\pm4}$	60 ± 2	-	-	-	-	$22{\scriptstyle~\pm2}$	50 ± 5	65 ± 2	55 ± 2

¹ Due to the high computational cost of pixel-based tasks, we selectively benchmark 5 methods that achieve strong performance on state-based OGBench tasks.

Table 2: **Offline-to-online RL results.** Following FQL (Park, Li, and Levine 2025), the results are obtained by first training the policy offline for 1M steps and subsequently performing online fine-tuning.

Task	IQL	ReBRAC	Cal-QL	RLPD	IFQL	FQL	Ours
antmaze-giant-navigate	$2 \pm 1 \rightarrow 3 \pm 1$	$6 \pm 5 \rightarrow 34 \pm 4$	$0 \pm 0 \rightarrow 0 \pm 0$	$0 \pm_0 \rightarrow 48 \pm_{13}$	$0 \pm_0 \to 69 \pm_{12}$	$4 \pm_2 \rightarrow 9 \pm_3$	$0 \pm_0 \rightarrow 82 \pm_5$
humanoidmaze-medium-navigate	$21 \pm 13 \rightarrow 16 \pm 8$	$16 \pm_{20} \rightarrow 1 \pm_{1}$	$0 \pm 0 \rightarrow 0 \pm 0$	$0 \pm 0 \rightarrow 8 \pm 10$	$56 \pm 35 \rightarrow 82 \pm 20$	$12 \pm 7 \rightarrow 22 \pm 12$	62 ±1 \rightarrow 100 ±1
antsoccer-arena-navigate	$2 \pm 1 \rightarrow 0 \pm 0$	$0 \pm 0 \rightarrow 0 \pm 0$	$0 \pm 0 \rightarrow 0 \pm 0$	$0 \pm 0 \rightarrow 0 \pm 0$	$26 \pm 15 \rightarrow 39 \pm 10$	$28 \pm 8 \rightarrow 86 \pm 5$	$62 \pm 3 \rightarrow 87 \pm 5$
cube-double-play	$0 \pm 1 \rightarrow 0 \pm 0$	$6 \pm 5 \rightarrow 28 \pm 28$	$0 \pm 0 \rightarrow 0 \pm 0$	$0 \pm 0 \rightarrow 0 \pm 0$	$12 \pm 9 \rightarrow 40 \pm 5$	$40 \pm_{11} \rightarrow 92 \pm_{3}$	$3 \pm_2 \rightarrow 95 \pm_2$
scene-play	$14 \pm 11 \rightarrow 10 \pm 9$	$55 \pm_{10} \rightarrow 100 \pm_{0}$	$1 \pm_2 \rightarrow 50 \pm_{53}$	$0 \pm_0 \rightarrow 100 \pm_0$	$0 \pm_1 \to 60 \pm_{39}$	$82 \pm 11 \rightarrow 100 \pm 1$	$60 \pm_1 \rightarrow 100 \pm_1$
puzzle-4x4-play	$5 \pm_2 \rightarrow 1 \pm_1$	$8 \pm {\scriptscriptstyle 4} \rightarrow 14 \pm {\scriptscriptstyle 35}$	$0 \pm 0 \rightarrow 0 \pm 0$	$0 \pm_0 \rightarrow 100 \pm_1$	$23~{\scriptstyle \pm 6} \rightarrow 19~{\scriptstyle \pm 33}$	$8 \pm {\scriptscriptstyle 3} \rightarrow 38 \pm {\scriptscriptstyle 52}$	$40 \pm_6 \rightarrow 100 \pm_1$
antmaze-umaze-v2	$77 \rightarrow 96$	$98 \rightarrow 75$	77 ightarrow 100	$0 \pm_0 \to 98 \pm_3$	$94 \pm_5 \to 96 \pm_2$	$97 \pm_2 \rightarrow 99 \pm_1$	$98 \pm_1 \rightarrow 99 \pm_1$
antmaze-umaze-diverse-v2	$60 \rightarrow 64$	$74 \rightarrow 98$	$32 \rightarrow 98$	$0 \pm 0 \rightarrow 94 \pm 5$	$69 \pm_{20} \to 93 \pm_{5}$	$79 \pm_{16} \rightarrow 100 \pm_{1}$	$79 \pm_2 \rightarrow 100 \pm_1$
antmaze-medium-play-v2	$72 \rightarrow 90$	$88 \rightarrow 98$	$72 \rightarrow 99$	$0 \pm_0 \to 98 \pm_2$	$52 \pm 19 \rightarrow 93 \pm 2$	77 $\pm 7 \to 97 \pm 2$	$86 \pm_2 \to 99 \pm_1$
antmaze-medium-diverse-v2	$64 \rightarrow 92$	$85 \rightarrow 99$	$62 \rightarrow 98$	$0 \pm_0 \to 97 \pm_2$	$44 \pm 26 \rightarrow 89 \pm 4$	$55 \pm_{19} \rightarrow 97 \pm_{3}$	$78 \pm_2 \rightarrow 99 \pm_2$
antmaze-large-play-v2	$38 \rightarrow 64$	$68 \rightarrow 32$	$32 \rightarrow 97$	$0 \pm_0 \to 93 \pm_5$	$64 \pm 14 \rightarrow 80 \pm 5$	$66 \pm 40 \rightarrow 84 \pm 30$	$80 \pm 3 \rightarrow 94 \pm 4$
antmaze-large-diverse-v2	$27 \rightarrow 64$	$67 \rightarrow 72$	44 o 92	$0 \pm_0 \rightarrow 94 \pm_3$	$69~{\scriptstyle \pm 6} \rightarrow 86~{\scriptstyle \pm 5}$	$75 \pm 24 \rightarrow 94 \pm 3$	$76~{\scriptstyle \pm 1} \rightarrow 96~{\scriptstyle \pm 3}$
pen-cloned-v1	$84 \rightarrow 102$	$74 \rightarrow 138$	$-3 \rightarrow -3$	$3 \pm_2 \rightarrow 120 \pm_{10}$	$77 \pm 7 \rightarrow 107 \pm 10$	$53 \pm 14 \rightarrow 149 \pm 6$	$79 \pm 3 \rightarrow $ 151 ± 7
door-cloned-v1	$1 \rightarrow 20$	$0 \rightarrow 102$	$0 \rightarrow 0$	$0 \pm_0 \to 102 \pm_7$	$3 \pm_2 \rightarrow 50 \pm_{15}$	$0 \pm_0 \to 102 \pm_5$	$3 \pm 1 \rightarrow 96 \pm 4$
hammer-cloned-v1	$1 \rightarrow 57$	$7 \rightarrow 125$	$0 \rightarrow 0$	$0 \pm_0 \rightarrow 128 \pm_{29}$	$4 \pm_2 \rightarrow 60 \pm_{14}$	$0 \pm 0 \rightarrow 127 \pm 17$	$10 \pm 5 \rightarrow 132 \pm 11$
relocate-cloned-v1	$0 \rightarrow 0$	$1 \rightarrow 7$	$0 \rightarrow 0$	$0 \pm 0 \rightarrow 2 \pm 2$	$0 \pm 0 \rightarrow 5 \pm 3$	$0 \pm 1 \rightarrow 62 \pm 8$	$1 \; {\scriptstyle \pm 1} \rightarrow 19 \; {\scriptstyle \pm 8}$

These results highlight the robustness and sample efficiency of our approach when transitioning from offline training to online adaptation. Notably, these improvements are obtained without any modifications to the model architecture or training objective, allowing the policy to interact with the environment in a more reward-sensitive and direct manner. This unified design facilitates more effective exploration, which is critical for rapid adaptation from offline to online. Overall, the strong performance of our generative policy in both static and interactive settings highlights its potential for real-world deployment in evolving environments.

Further Analysis

Our method vs naive MeanFlow. To evaluate the effectiveness of our proposed reformulation strategy, we compare it against the original MeanFlow framework under the same environment and with well-tuned hyperparameters. As shown in Fig. 3, the naive MeanFlow approach demonstrates performance (left) and flow loss (mid.) metrics that are nearly indistinguishable from ours during the initial stages of training. However, the bound loss (right) metric—defined as the mean absolute magnitude of action values outside [-1,1]—is substantially higher for the naive MeanFlow approach. This indicates it predicts actions not in the valid range. Thus, its performance then degrades significantly due to inaccurate Q-

value estimates from the critic, which impair the training of the generative flow model and result in a low success rate.

Analysis of coefficient α in policy learning. The hyperparameter α controls the relative strength of the behaviour cloning term versus the Q-function objective in the training loss. As shown in Fig. 4, overly small values of α lead to unstable updates due to over-reliance on potentially noisy Q estimates, while overly large values lead to simply behaviour cloning learning. Specifically, although we employ an adaptive α tuning mechanism in our main experiments, the model's final performance still exhibits sensitivity to initial α values, especially in sparse-reward tasks, e.g. Puzzle3x3. This highlights the importance of a balanced trade-off, and motivates future research on more robust adaptive schemes.

To further examine the sensitivity of our method to the coefficient α , we analyze its evolution during training under the proposed adaptive adjustment strategy. As shown in Fig. 5, we can see α evolves smoothly and remains well-regulated throughout learning based on our adaptive mechanism. This dynamic adaptation effectively balances the trade-off between behaviour cloning and value maximisation, thereby enhancing the robustness of our method across different training stages and contributing to our superior performance over FQL (Park, Li, and Levine 2025).

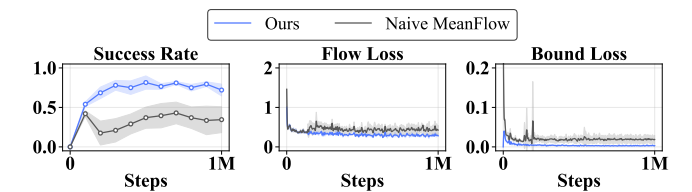


Figure 3: Comparison of learning curves. Naive MeanFlow exhibits significantly larger bound losses in the early training stages. This instability directly undermines convergence of its flow loss, leading to a substantial performance gap compared to ours on the antsoccer-arena-singletask.

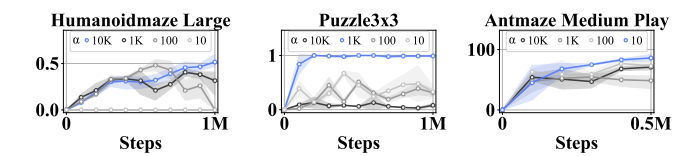


Figure 4: Sensitivity to the behaviour cloning coefficient α . Effect of different values of α on offline RL performance.

Effect of candidate size K in value-guided selection. In our value-guided rejection sampling, hyperparameter K controls the number of candidate actions generated and scored by the Q-function for each state. As shown in Fig. 6, we observe that increasing K from 1 to 5 leads to a substantial performance gain across various tasks. However, setting K too large (e.g., 20) may impair performance by reducing stochasticity and exploration diversity, as overly greedy selection can cause the critic function to focus on a narrow set of high-value actions, thereby limiting behavioural variability. In practice, we find that K=5 offers the best trade-off, preserving policy exploration and maintaining computational efficiency.

Related Works

Generalised behaviour cloning. Behaviour cloning (BC) casts policy learning as a supervised task over expert stateaction pairs (Hussein et al. 2017; Block et al. 2023). Generalised variants, such as advantage-weighted imitation (Peters and Schaal 2007), steer learning toward high-return trajectories by weighting actions by their cumulative rewards. Recent methods extend this idea in different ways: SfBC (Chen et al. 2023b) and IDQL (Hansen-Estruch et al. 2023) pretrain a behaviour policy and critic to support importance sampling; OGPO (Lu et al. 2023) distills the critic into an energybased model; GMPO and GMPG (Zhang et al. 2024) apply weighted policy gradient updates directly without pretraining; and QIPO (Zhang, Zhang, and Gu 2025) incorporates Q-value-derived energy into flow-matching updates. Despite these advances, recent studies highlight their inefficiency and limited performance in complex tasks (Park et al. 2024).

Generative policy with Q-learning. Incorporating Q-functions into generative policies, enabling direct reward-driven optimisation, offers a more principled alternative to behaviour cloning. These works often optimise policies with Q-learning by differentiating through the generative model's reverse process. Methods such as DQL (Wang, Hunt,

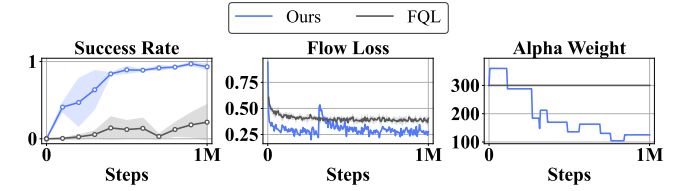


Figure 5: Training dynamics under our framework in humanoidmaze-large-navigate-singletask. Despite potential sensitivity, the adaptive coefficient α adjusts dynamically and evolves smoothly, contributing to stable and robust policy learning throughout the training process.

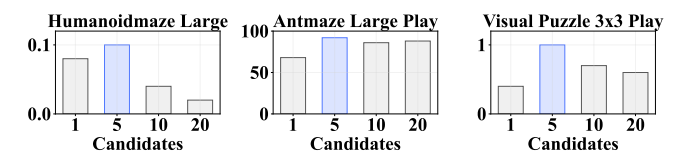


Figure 6: Performance effect of candidates num. K used in value-guided rejection sampling on three representative tasks.

and Zhou 2022), Consistency-AC (Ding and Jin 2024), and DACER (Wang et al. 2024) perform policy improvement via reverse diffusion, but suffer from high computational cost due to repeated denoising and unrolled optimisation.

To alleviate this, one-step generative policies have recently been proposed to avoid iterative sampling (Chen et al. 2024; Prasad et al. 2024; Koirala and Fleming 2025). Existing approaches follow two main directions: distillation-based methods that compress multi-step teachers into one-step student policies (Chen et al. 2023a; Park, Li, and Levine 2025), and algorithmic innovations that enable direct action generation. such as consistency (Song et al. 2023) and shortcut (Frans et al. 2025) models. Among them, FQL (Park, Li, and Levine 2025) distils a flow-based policy into a one-step model optimised with Q-learning, while SORL (Espinosa-Dice et al. 2025) leverages shortcut frameworks (Frans et al. 2025) to flexibly scale training and inference. However, both methods either rely on multi-stage pipelines or require inference-time scaling to achieve strong performance, thus falling short of a fully effective one-step policy learning framework.

Conclusion

We propose a one-step generative framework for offline RL that enables expressive and stable policy learning without relying on multi-step integration or policy distillation. Through a residual reformulation of MeanFlow, our method supports direct Q-learning with multimodal policies via a single-stage training pipeline. To further improve performance and robustness, we incorporate value-guided rejection sampling and adaptive behaviour cloning regularisation. Experiment results show our method outperforming or matching prior work on most of the 73 tasks and reaching state-of-the-art performance on nearly all offline-to-online transfers, highlighting robust generalisation and adaptation. Overall, this work bridges the gap between one-step generative modelling and value-based reinforcement learning, advancing the development of more expressive and scalable offline policy learning.

Acknowledgments

This work was supported in part by the National Natural Science Foundation of China under Grant No. 62206305. Zeyuan Wang completed this work during the author's visiting study at the Shanghai Innovation Institute, whose support are gratefully acknowledged. Prof. Yanwei Fu was partly supported by the project from the Ministry of Science and Higher Education of the Republic of Kazakhstan, No. BR24992975, 'Development of a digital twin of a food processing enterprise using artificial intelligence and IIoT technologies' (2024–2026).

References

- Adam, K. D. B. J.; et al. 2014. A method for stochastic optimization. *arXiv preprint arXiv:1412.6980*, 1412(6).
- Ball, P. J.; Smith, L.; Kostrikov, I.; and Levine, S. 2023. Efficient online reinforcement learning with offline data. In *International Conference on Machine Learning (ICML)*.
- Block, A.; Jadbabaie, A.; Pfrommer, D.; Simchowitz, M.; and Tedrake, R. 2023. Provable guarantees for generative behavior cloning: Bridging low-level stability and high-level behavior. *Advances in Neural Information Processing Systems (NeurIPS)*.
- Bradbury, J.; Frostig, R.; Hawkins, P.; Johnson, M. J.; Leary, C.; Maclaurin, D.; Necula, G.; Paszke, A.; VanderPlas, J.; Wanderman-Milne, S.; et al. 2018. JAX: composable transformations of Python+ NumPy programs.
- Chen, H.; Lu, C.; Wang, Z.; Su, H.; and Zhu, J. 2023a. Score regularized policy optimization through diffusion behavior. *arXiv preprint arXiv:2310.07297*.
- Chen, H.; Lu, C.; Ying, C.; Su, H.; and Zhu, J. 2023b. Offline Reinforcement Learning via High-Fidelity Generative Behavior Modeling. In *The Eleventh International Conference on Learning Representations (ICLR)*.
- Chen, J.; Ganguly, B.; Xu, Y.; Mei, Y.; Lan, T.; and Aggarwal, V. 2024. Deep generative models for offline policy learning: Tutorial, survey, and perspectives on future directions. *arXiv* preprint arXiv:2402.13777.
- Chen, T.; Wang, Z.; and Zhou, M. 2024. Diffusion policies creating a trust region for offline reinforcement learning. *Advances in Neural Information Processing Systems (NeurIPS)*.
- Chi, C.; Xu, Z.; Feng, S.; Cousineau, E.; Du, Y.; Burchfiel, B.; Tedrake, R.; and Song, S. 2023. Diffusion policy: Visuomotor policy learning via action diffusion. *The International Journal of Robotics Research*.
- Ding, Z.; and Jin, C. 2024. Consistency models as a rich and efficient policy class for reinforcement learning. In *12th International Conference on Learning Representations (ICLR)*. Espinosa-Dice, N.; Zhang, Y.; Chen, Y.; Guo, B.; Oertell, O.; Swamy, G.; Brantley, K.; and Sun, W. 2025. Scaling Offline RL via Efficient and Expressive Shortcut Models. *arXiv* preprint arXiv:2505.22866.
- Esser, P.; Kulal, S.; Blattmann, A.; Entezari, R.; Müller, J.; Saini, H.; Levi, Y.; Lorenz, D.; Sauer, A.; Boesel, F.; et al. 2024. Scaling rectified flow transformers for high-resolution image synthesis. In *Forty-first International conference on machine learning (ICML)*.

- Frans, K.; Hafner, D.; Levine, S.; and Abbeel, P. 2025. One Step Diffusion via Shortcut Models. In *The Thirteenth International Conference on Learning Representations (ICLR)*.
- Fu, J.; Kumar, A.; Nachum, O.; Tucker, G.; and Levine, S. 2020. D4rl: Datasets for deep data-driven reinforcement learning. *arXiv* preprint arXiv:2004.07219.
- Geng, Z.; Deng, M.; Bai, X.; Kolter, J. Z.; and He, K. 2025. Mean flows for one-step generative modeling. *arXiv preprint arXiv:2505.13447*.
- Hafner, R.; and Riedmiller, M. 2011. Reinforcement learning in feedback control. *Machine Learning*.
- Hansen-Estruch, P.; Kostrikov, I.; Janner, M.; Kuba, J. G.; and Levine, S. 2023. Idql: Implicit q-learning as an actor-critic method with diffusion policies. *arXiv preprint arXiv:2304.10573*.
- Hussein, A.; Gaber, M. M.; Elyan, E.; and Jayne, C. 2017. Imitation learning: A survey of learning methods. *ACM Computing Surveys (CSUR)*.
- Jin, Y.; Sun, Z.; Li, N.; Xu, K.; Xu, K.; Jiang, H.; Zhuang, N.; Huang, Q.; Song, Y.; MU, Y.; and Lin, Z. 2025. Pyramidal Flow Matching for Efficient Video Generative Modeling. In *The Thirteenth International Conference on Learning Representations (ICLR)*.
- Koirala, P.; and Fleming, C. 2025. Flow-Based Single-Step Completion for Efficient and Expressive Policy Learning. *arXiv* preprint arXiv:2506.21427.
- Kostrikov, I.; Nair, A.; and Levine, S. 2021. Offline Reinforcement Learning with Implicit Q-Learning. In *Deep RL Workshop NeurIPS 2021*.
- Leshno, M.; Lin, V. Y.; Pinkus, A.; and Schocken, S. 1993. Multilayer feedforward networks with a nonpolynomial activation function can approximate any function. *Neural networks*.
- Lipman, Y.; Chen, R. T.; Ben-Hamu, H.; Nickel, M.; and Le, M. 2023. Flow Matching for Generative Modeling. In 11th International Conference on Learning Representations (ICLR).
- Liu, A. H.; Le, M.; Vyas, A.; Shi, B.; Tjandra, A.; and Hsu, W.-N. 2024. Generative Pre-training for Speech with Flow Matching. In *The Twelfth International Conference on Learning Representations (ICLR)*.
- Liu, X.; Gong, C.; and Liu, Q. 2023. Flow Straight and Fast: Learning to Generate and Transfer Data with Rectified Flow. In *The Eleventh International Conference on Learning Representations (ICLR)*.
- Lu, C.; Chen, H.; Chen, J.; Su, H.; Li, C.; and Zhu, J. 2023. Contrastive energy prediction for exact energy-guided diffusion sampling in offline reinforcement learning.
- Mees, O.; Ghosh, D.; Pertsch, K.; Black, K.; Walke, H. R.; Dasari, S.; Hejna, J.; Kreiman, T.; Xu, C.; Luo, J.; et al. 2024. Octo: An open-source generalist robot policy. In *First Workshop on Vision-Language Models for Navigation and Manipulation at ICRA*.
- Nair, A.; Gupta, A.; Dalal, M.; and Levine, S. 2020. Awac: Accelerating online reinforcement learning with offline datasets. *arXiv preprint arXiv:2006.09359*.

- Nakamoto, M.; Zhai, S.; Singh, A.; Sobol Mark, M.; Ma, Y.; Finn, C.; Kumar, A.; and Levine, S. 2023. Cal-ql: Calibrated offline rl pre-training for efficient online fine-tuning. *Advances in Neural Information Processing Systems (NeurIPS)*.
- O'Neill, A.; Rehman, A.; Maddukuri, A.; Gupta, A.; Padalkar, A.; Lee, A.; Pooley, A.; Gupta, A.; Mandlekar, A.; Jain, A.; et al. 2024. Open x-embodiment: Robotic learning datasets and rt-x models: Open x-embodiment collaboration 0. In 2024 IEEE International Conference on Robotics and Automation (ICRA).
- Park, S.; Frans, K.; Eysenbach, B.; and Levine, S. 2025. OG-Bench: Benchmarking Offline Goal-Conditioned RL. In *The Thirteenth International Conference on Learning Representations (ICLR)*.
- Park, S.; Frans, K.; Levine, S.; and Kumar, A. 2024. Is value learning really the main bottleneck in offline RL? *Advances in Neural Information Processing Systems (NeurIPS)*.
- Park, S.; Li, Q.; and Levine, S. 2025. Flow Q-Learning. In *Forty-second International conference on machine learning (ICML)*.
- Peebles, W.; and Xie, S. 2023. Scalable diffusion models with transformers. In *Proceedings of the IEEE/CVF international conference on computer vision (ICCV)*, 4195–4205.
- Peters, J.; and Schaal, S. 2007. Reinforcement learning by reward-weighted regression for operational space control. In *Proceedings of the 24th International conference on machine learning (ICML)*.
- Pomerleau, D. A. 1988. Alvinn: An autonomous land vehicle in a neural network. *Advances in Neural Information Processing Systems (NeurIPS)*.
- Prasad, A.; Lin, K.; Wu, J.; Zhou, L.; and Bohg, J. 2024. Consistency Policy: Accelerated Visuomotor Policies via Consistency Distillation. *CoRR*.
- Puterman, M. L. 2014. *Markov decision processes: discrete stochastic dynamic programming*. John Wiley & Sons.
- Quinton, P.; and Rey, V. 2024. Jacobian descent for multi-objective optimization. *arXiv preprint arXiv:2406.16232*.
- Schulman, J.; Wolski, F.; Dhariwal, P.; Radford, A.; and Klimov, O. 2017. Proximal policy optimization algorithms. *arXiv preprint arXiv:1707.06347*.
- Sheng, J.; Wang, Z.; Li, P.; and Liu, M. 2025. MP1: Mean Flow Tames Policy Learning in 1-step for Robotic Manipulation. *arXiv* preprint arXiv:2507.10543.
- Song, Y.; Dhariwal, P.; Chen, M.; and Sutskever, I. 2023. Consistency Models. In *International conference on machine learning (ICML)*.
- Song, Y.; and Prafulla, D. 2024. Improved Techniques for Training Consistency Models. In *12th International Conference on Learning Representations (ICLR)*.
- Sutton, R. S.; Barto, A. G.; et al. 1998. *Reinforcement learning: An introduction*, volume 1. MIT press Cambridge.
- Tabuada, P.; and Gharesifard, B. 2021. Universal approximation power of deep residual neural networks via nonlinear control theory. In *International Conference on Learning Representations (ICLR)*.

- Tarasov, D.; Kurenkov, V.; Nikulin, A.; and Kolesnikov, S. 2023a. Revisiting the minimalist approach to offline reinforcement learning. *Advances in Neural Information Processing Systems (NeurIPS)*.
- Tarasov, D.; Nikulin, A.; Akimov, D.; Kurenkov, V.; and Kolesnikov, S. 2023b. CORL: Research-oriented deep offline reinforcement learning library. *Advances in Neural Information Processing Systems (NeurIPS)*.
- Vaswani, A.; Shazeer, N.; Parmar, N.; Uszkoreit, J.; Jones, L.; Gomez, A. N.; Kaiser, Ł.; and Polosukhin, I. 2017. Attention is all you need. *Advances in neural information processing systems (NeurIPS)*.
- Wang, Y.; Wang, L.; Jiang, Y.; Zou, W.; Liu, T.; Song, X.; Wang, W.; Xiao, L.; Wu, J.; Duan, J.; et al. 2024. Diffusion actor-critic with entropy regulator. *Advances in Neural Information Processing Systems (NeurIPS)*.
- Wang, Z.; Hunt, J. J.; and Zhou, M. 2022. Diffusion policies as an expressive policy class for offline reinforcement learning. *arXiv* preprint arXiv:2208.06193.
- Zhang, J.; Xue, R.; Niu, Y.; Chen, Y.; Yang, J.; Li, H.; and Liu, Y. 2024. Revisiting Generative Policies: A Simpler Reinforcement Learning Algorithmic Perspective. *arXiv* preprint arXiv:2412.01245.
- Zhang, Q.; Liu, Z.; Fan, H.; Liu, G.; Zeng, B.; and Liu, S. 2025. Flowpolicy: Enabling fast and robust 3d flow-based policy via consistency flow matching for robot manipulation. In *Proceedings of the AAAI Conference on Artificial Intelligence (AAAI)*.
- Zhang, S.; Zhang, W.; and Gu, Q. 2025. Energy-weighted flow matching for offline reinforcement learning. *arXiv* preprint arXiv:2503.04975.

Appendix

A Limitations

Despite promising results, our method has several limitations. First, the final performance remains sensitive to the choice of the hyperparameter α , which balances the behaviour cloning loss and the Q-value objective. Although we introduce an adaptive scheme for tuning α , it does not fully eliminate the need for hyperparameter search, and the optimal value may still vary across tasks. Future work could explore multi-objective optimisation techniques (such as Jacobian Descent (Quinton and Rey 2024)) to better balance these competing objectives. Second, our method relies on the MeanFlow formulation, which requires computing Jacobian-vector products (JVPs (Bradbury et al. 2018)) during training. While this enables efficient one-step flow-based modelling, it can introduce additional computational overhead, potentially affecting training speed in large-scale settings. We consider addressing these issues as promising directions for future work.

B Remedies for Action Clipping in One-Step Flow-Based Q-Learning Policies

In its original form, MeanFlow generates an action by subtracting a learned velocity from a sample of Gaussian noise in one-step like:

$$\hat{a} = e - u(e, b=0, t=1)$$
 (22)

where $e \sim \mathcal{N}(0, I)$ represents random noise, and u is a neural network trained to predict an *average velocity* vector. Although this formulation allows actions to be sampled without iterative integration over time, it suffers from a key drawback: since the noise e is unbounded, the resulting action \hat{a} often lies outside the valid action range (typically [-1,1]). This issue is especially pronounced early in training, when the learned velocity u is still inaccurate. As a result, actions are frequently clipped back into the valid range, which breaks the alignment between the policy's outputs and the Q-function's targets, leading to unstable and inefficient learning.

A natural way to mitigate the issue of out-of-bound actions is to ensure that the final output of the generative model remains within the valid action range (e.g., [-1, 1]). Broadly, two strategies can be employed to achieve this goal.

The first approach is to constrain the output through a suitable activation function (such as tanh) applied at the end of the network. This guarantees bounded actions without the need for post-hoc clipping, thus preserving gradient consistency and improving stability during training.

The second, more direct approach is to replace the residual formulation entirely and train a model that maps the noise vector e directly to an action a, i.e., learning a function $f_{\theta}: e \mapsto a$ that generates valid actions by design. This formulation avoids both explicit velocity modelling and action correction, offering a simpler forward process. We will discuss these two simple and direct solution in detail as follows:

B.1 The Limitations of Gradient Distortion in Activation Mappings In the original MeanFlow formulation, actions are generated via a subtraction operation a = e - u, where e is sampled from a standard Gaussian and u is a learned average velocity. However, since e is unbounded, the resulting action a may fall outside the valid action range (e.g., [-1,1]). A common workaround is to apply hard clipping post-hoc, but this introduces discontinuities in the gradient flow and leads to gradient distortion during training.

To resolve this issue, we adopt a smooth bounding strategy based on the *softsign* activation function. A natural idea is to directly apply softsign to the output e - u:

$$a = \operatorname{softsign}(e - u) = \frac{e - u}{1 + |e - u|}$$
(23)

which smoothly squashes the unbounded input into the range (-1,1), thereby avoiding invalid actions and eliminating the need for hard clipping. However, this also means the model no longer directly learns the true action a, but rather a transformed version of it, which may impede expressivity or stability.

To address this, we instead apply the inverse of the softsign function during training. Specifically, given a target action $a \in [-1, 1]$, we compute its approximate inverse:

action_inv = inv_softsign(a) =
$$\frac{a}{1 - |a| + \varepsilon}$$
 (24)

where ε is a small constant for numerical stability. The model is then trained to predict action_inv in the unconstrained space, and the final action is recovered via a forward softsign transformation:

$$a = softsign(action_inv)$$
 (25)

This design ensures that the model output always lies within valid bounds, while retaining a smooth, differentiable mapping and avoiding post-hoc clipping. Moreover, it preserves the expressivity of the learned actions by decoupling the bounded constraint from the learning target.

Figure 7 visualizes both the softsign function and its inverse. The softsign curve demonstrates smooth saturation as input magnitude increases, while the inverse function expands the bounded action back into an unbounded domain. Together, they form a stable and differentiable mapping pair for generative policies.

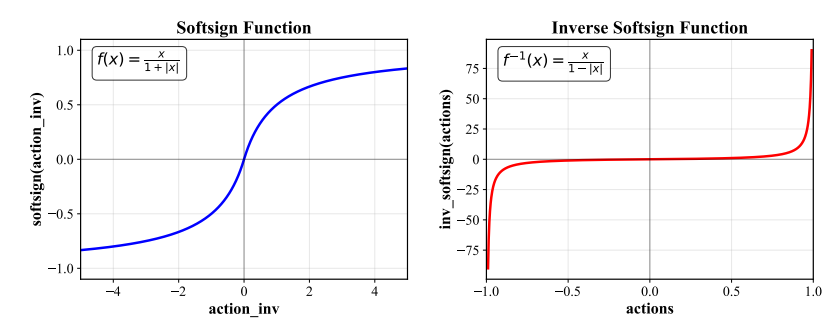


Figure 7: Visualization of the forward and inverse softsign transformations. Left: the softsign function smoothly bounds unbounded inputs to (-1, 1). Right: the approximate inverse inv_softsign restores an unbounded representation, enabling consistent bidirectional mappings for policy learning.

Although the forward-inverse pair formed by the softsign and its approximate inverse exhibits appealing mathematical properties—particularly the ability to perform smooth, lossless value transformations in the numerical sense—the empirical performance of this approach in policy learning remains suboptimal. The key limitation arises not from the value-preserving nature of the transformation, but from its *gradient distortion*.

While the transformation $a = \operatorname{softsign}(x)$ is numerically invertible, its gradient $\frac{d \operatorname{softsign}(x)}{dx} = \frac{1}{(1+|x|)^2}$ is highly non-uniform across the input space. Near the origin (i.e., $x \approx 0$), the gradient remains relatively large and stable. However, as x increases in magnitude, the gradient rapidly diminishes. This imbalance means that inputs near the saturation region (e.g., when $|x| \to 5$) contribute far less to the gradient signal during backpropagation.

More problematically, when performing the inverse mapping $x=\text{inv_softsign}(a)$, the gradient $\frac{d \, \text{inv_softsign}(a)}{da} = \frac{1}{(1-|a|+\varepsilon)^2}$ becomes sharply amplified as $|a| \to 1$. As a result, actions near the boundary (i.e., $a \approx \pm 1$) dominate the gradient update, leading the model to prefer generating actions near the extremes. This skewed gradient flow introduces significant training instability and mode collapse around the action boundaries, ultimately undermining the policy's expressivity and performance.

Therefore, despite its smoothness and reversibility, the softsign-based activation strategy suffers from a mismatch between forward stability and backward learning dynamics—a mismatch that proves detrimental in practice.

B.2 The Pitfall of Simple Residual Substitution Another natural extension of MeanFlow is to explicitly define a residual mapping from noise to action by setting:

$$g_{\theta}(a_t, b, t) = e - u_{\theta}(e, b, t), \tag{26}$$

where u(e, b, t) denotes the average velocity field. This reformulation enables single-stage action generation while preserving the underlying structure of MeanFlow.

To derive the training objective for g, we begin from the *MeanFlow Identity* (Geng et al. 2025), which defines the average velocity as:

$$(t-b) \cdot u(a_t, b, t) \triangleq \int_b^t v(a_\tau, \tau) \, d\tau, \tag{27}$$

where $a_t = (1 - t) \cdot a + t \cdot e$, and v denotes the instantaneous velocity field.

Based on this identity, we derive the regression target to supervise the learning of g_{θ} . Differentiating both sides of Equation 27 with respect to t, we obtain:

$$u(a_t, b, t) + (t - b) \cdot \frac{d}{dt} u(a_t, b, t) = v(a_t, t).$$
 (28)

Substituting $u(e, b, t) = e - g(a_t, b, t)$ into Equation 28 yields:

$$(e - g(a_t, b, t)) + (t - b) \cdot \frac{d}{dt} (e - g(a_t, b, t)) = v(a_t, t)$$

$$\Rightarrow e - g(a_t, b, t) - (t - b) \cdot \frac{d}{dt} g(a_t, b, t) = v(a_t, t).$$
(29)

Rearranging terms, we arrive at a key identity for the residual function:

$$g(a_t, b, t) = e - v(a_t, t) + (t - b) \cdot \frac{d}{dt} g(a_t, b, t).$$
(30)

To expand the total derivative $\frac{d}{dt}g(a_t,b,t)$, we apply the chain rule:

$$\frac{d}{dt}g(a_t, b, t) = \frac{da_t}{dt} \cdot \partial_{a_t}g + \frac{db}{dt} \cdot \partial_b g + \frac{dt}{dt} \cdot \partial_t g. \tag{31}$$

Given $a_t = (1-t)a + te$, we have $\frac{da_t}{dt} = e - a = v(a_t, t)$, $\frac{db}{dt} = 0$, and $\frac{dt}{dt} = 1$. Thus:

$$\frac{d}{dt}g(a_t, b, t) = v(a_t, t) \cdot \partial_{a_t}g + \partial_t g. \tag{32}$$

Substituting Equation 32 into Equation 30, we obtain the final regression target:

$$g_{tgt} = e - v(a_t, t) + (t - b) [v(a_t, t) \cdot \partial_{a_t} g + \partial_t g] = a + (t - b) [v(a_t, t) \cdot \partial_{a_t} g + \partial_t g].$$
(33)

We now parameterize g_{θ} as a neural network and treat Equation 33 as a supervision signal for training. Specifically, we define a behaviour cloning loss to regress the predicted residuals toward their analytical targets:

$$\mathcal{L}_{BC}(\theta) = \mathbb{E} \left\| g_{\theta}(a_t, b, t) - \operatorname{sg}(g_{\text{tgt}}) \right\|_2^2, \tag{34}$$

where the target residual is given by:

$$g_{\text{tgt}} = a + (t - b) \left[v(a_t, t) \cdot \partial_{a_t} g + \partial_t g \right]. \tag{35}$$

This formulation seemingly preserves the theoretical foundation of MeanFlow while enabling efficient one-stage sampling. However, as we show in our toy dataset experiments in Figure 8, this residual substitution yields results that deviate significantly from our initial intuition, revealing nontrivial empirical mismatches despite its apparent theoretical appeal.

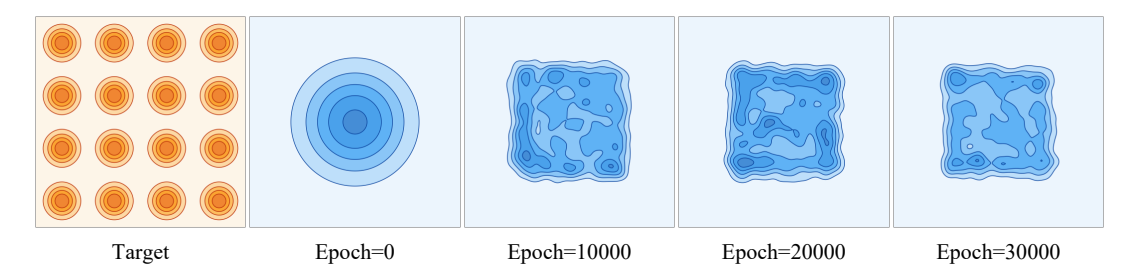


Figure 8: Training dynamics of the residual model $g_{\theta}(e) = e - u(e, b, t)$ on a 4×4 checkerboard distribution. From left to right: the target distribution and the model outputs at different training epochs (0, 10k, 20k, 30k). Although the residual mapping allows for single-stage sampling, the learned distribution fails to recover the desired multi-modal structure, revealing the limitations of directly modelling e - u.

B.3 Equivalent Reformulation of MeanFlow Given that both intuitive modifications—bounded activation functions and simple substitutions—fail to match the performance and generality of the original MeanFlow formulation, we are motivated to address the following question:

How can we construct a network that is both theoretically equivalent to MeanFlow and practically enables one-step noise-to-action generation?

To this end, we revisit the core structure of MeanFlow: its defining characteristic is the integration of a velocity field over time, which effectively captures a continuous flow from the noise vector e to the action a. Any alternative formulation that aims to preserve this behavior must replicate not only the mapping $e \mapsto a$, but also the intermediate dynamics and temporal consistency embedded in the original construction. Formally, we propose:

Remark. To enable direct one-step inference—where actions are deterministically generated from Gaussian noise—it is beneficial to enforce the following constraint:

$$\phi(e, b^*, t^*) = e, \quad \text{for some fixed } b^*, t^*, \tag{36}$$

where $e \sim \mathcal{N}(0, I)$.

Under this condition, the residual model satisfies:

$$q_{\theta}(e, b^*, t^*) = \phi(e, b^*, t^*) - u_{\theta}(e, b^*, t^*) = a,$$
 (37)

which enables tractable and controlled noise-to-action generation at a designated inference time step.

Design Rationale. To construct a residual formulation of the form

$$g_{\theta}(a_t, b, t) = \phi(a_t, b, t) - u_{\theta}(a_t, b, t),$$
 (38)

our goal is to preserve the expressive power and theoretical soundness of the original MeanFlow framework. This requires that the reformulation be both well-posed and learnable in practice. To this end, we identify two key properties that the residual ϕ must satisfy:

- ϕ should be fixed. To ensure a unique and interpretable decomposition, ϕ should be fixed and independent of the learnable component u_{θ} . If both components are trained jointly, the residual g_{θ} remains invariant under simultaneous perturbations of ϕ and u_{θ} , resulting in a degenerate solution space and entangled gradients. Fixing ϕ eliminates this ambiguity and leads to stable, well-defined optimisation.
- ϕ should be analytic. In temporally evolving settings—such as flow-based training along interpolated trajectories—differentiability with respect to time is essential. If ϕ lacks regularity, the required derivatives may become ill-defined or unstable. Requiring ϕ to be analytic ensures smooth gradient propagation and coherent temporal behavior.

Together, these two desiderata motivate a sufficient condition: ϕ should be a fixed, analytic function with respect to its input variables (a_t, b, t) , defined over a compact domain. The following proposition formalizes this condition and demonstrates that it preserves the expressive capacity of the residual formulation.

Proposition (Sufficiency). Let the residual parameterization be defined as

$$g_{\theta}(a_t, b, t) = \phi(a_t, b, t) - u_{\theta}(a_t, b, t),$$
 (39)

where $\phi \colon \mathcal{X} \to \mathbb{R}^d$ is a fixed, analytic function independent of the learnable component u_{θ} , and $\mathcal{X} \subset \mathbb{R}^m$ is a compact domain. Then, for any target function $h \in \mathcal{C}(\mathcal{X}; \mathbb{R}^d)$, there exists a neural network $u_{\theta} \colon \mathcal{X} \to \mathbb{R}^d$ such that the residual form $g_{\theta} = \phi - u_{\theta}$ approximates h arbitrarily well in the uniform norm.

Proof. Let $h \in \mathcal{C}(\mathcal{X}; \mathbb{R}^d)$ be an arbitrary continuous target function. Define the corresponding residual target:

$$u^*(x) := \phi(x) - h(x), \text{ where } x := (a_t, b, t) \in \mathcal{X}.$$
 (40)

Since both ϕ and h are continuous on the compact domain \mathcal{X} , their difference u^* is also continuous, i.e., $u^* \in \mathcal{C}(\mathcal{X}; \mathbb{R}^d)$.

By the universal approximation theorem (Leshno et al. 1993), for any $\varepsilon > 0$, there exists a neural network $u_{\theta} \colon \mathcal{X} \to \mathbb{R}^d$ such that

$$\sup_{x \in \mathcal{X}} \|u_{\theta}(x) - u^*(x)\| < \varepsilon. \tag{41}$$

Substituting into the residual formulation $q_{\theta}(x) = \phi(x) - u_{\theta}(x)$, we obtain:

$$||g_{\theta}(x) - h(x)|| = ||\phi(x) - u_{\theta}(x) - h(x)||$$

= $||u^*(x) - u_{\theta}(x)|| < \varepsilon, \quad \forall x \in \mathcal{X}.$ (42)

Hence, the residual function $q_{\theta} = \phi - u_{\theta}$ uniformly approximates the target $h = \phi - u^*$ on \mathcal{X} .

Conclusion. We conclude that:

 $\phi(a_t, b, t)$ is a fixed, analytic function of the input variables, independent of θ

$$\Rightarrow q_{\theta}(a_t, b, t) = \phi(a_t, b, t) - u_{\theta}(a_t, b, t)$$
 retains the expressivity of the original u_{θ} . (43)

Boundary Condition and Construction of ϕ **.** To enable a tractable and deterministic noise-to-action mapping at inference time, we seek a formulation where the residual output at b=0 and t=1 satisfies

$$q_{\theta}(e, 0, 1) = \phi(e, 0, 1) - u_{\theta}(e, 0, 1) \approx a,$$
 (44)

with $e \sim \mathcal{N}(0, I)$. This requirement can be fulfilled by choosing ϕ as a fixed, continuous (or analytic) function independent of the parameters θ , such that $\phi(e, 0, 1) = e$.

We adopt the simplest and most natural choice:

$$\phi(a_t, b, t) = a_t = (1 - t) \cdot a + t \cdot e, \tag{45}$$

which satisfies $\phi(e,0,1)=e$ under the standard linear interpolation schedule. Under this construction, the reformulation takes the form

$$g_{\theta}(a_t, b, t) = a_t - u_{\theta}(a_t, b, t), \tag{46}$$

and in particular:

$$g_{\theta}(e,0,1) = e - u_{\theta}(e,0,1) = a.$$
 (47)

This design, where ϕ is fixed, analytic, and independent of u_{θ} , ensures that the residual formulation $g_{\theta} = \phi - u_{\theta}$ retains the full expressivity of the original u_{θ} . Moreover, it enables efficient one-step sampling that remains consistent with the MeanFlow decoding identity under the boundary condition (b=0,t=1).

Analysis of Reformulation Variants. We revisit the design of reformulation schemes through the lens of our theoretical framework, particularly focusing on the validity of the residual form $g_{\theta} = \phi - u_{\theta}$. As summarized in Table 3, we explore several alternative formulations of the residual function in the form $g(a_t, b, t) = \phi(a_t, b, t) - u_{\theta}(a_t, b, t)$, each leading to a distinct training target. Below, we derive the corresponding target expressions and inference procedures for four representative variants.²

Variant 1: $\phi = a_t \Rightarrow g = a_t - u_\theta(a_t, b, t)$ Substituting the *MeanFlow Identity* into the definition of g, we have:

$$g(a_{t}, b, t) = a_{t} - u(a_{t}, b, t)$$

$$= a_{t} - \left[v(a_{t}, t) - (t - b) \cdot \frac{d}{dt}(a_{t} - g(a_{t}, b, t))\right]$$

$$= a_{t} - v(a_{t}, t) + (t - b)v(a_{t}, t) - (t - b) \cdot \frac{d}{dt}g(a_{t}, b, t).$$
(48)

We compute the total derivative of $g(a_t, b, t)$ with respect to t:

$$\frac{d}{dt}g(a_t, b, t) = v(a_t, t) \cdot \partial_{a_t}g + \partial_b g + \partial_t g = \text{jvp}(g, (a_t, b, t), (v, 0, 1)), \tag{49}$$

where jvp denotes the Jacobian-vector product along the temporal direction.

Substituting Equation 49 into the residual formulation and simplifying, we obtain the target residual:

$$g_{\text{tot}} = a_t + (t - b - 1)v(a_t, t) - (t - b) \cdot \text{jvp.}$$
 (50)

Inference: When b = 0, t = 1, the action can be directly recovered as:

$$a = e - u(e, 0, 1) = e - [a_t - g(e, 0, 1)] = g(e, 0, 1).$$
(51)

Variant 2: $\phi = 2 \Rightarrow g = 2 - u_{\theta}(a_t, b, t)$ Substituting *MeanFlow Identity* equation into the residual function:

$$g(a_{t}, b, t) = 2 - u(a_{t}, b, t)$$

$$= 2 - \left[v(a_{t}, t) - (t - b) \cdot \frac{d}{dt}(2 - g(a_{t}, b, t))\right]$$

$$= 2 - v(a_{t}, t) + (t - b) \cdot \left(-\frac{d}{dt}g(a_{t}, b, t)\right)$$

$$= 2 - v(a_{t}, t) - (t - b) \cdot \frac{d}{dt}g(a_{t}, b, t)$$
(52)

Substituting the total derivative (Equation 49) into the residual equation and regrouping terms, we can obtain:

$$g_{\text{tgt}} = 2 - v(a_t, t) - (t - b) \cdot \text{jvp}$$

$$\tag{53}$$

Inference: When b = 0, t = 1, the final action is recovered as:

$$a = e - u(e, 0, 1) = e - [2 - g(e, 0, 1)]$$
(54)

Variant 3: $\phi = t \Rightarrow q = t - u_{\theta}(t, b, t)$ Substituting *MeanFlow Identity* equation into the residual function:

$$g(a_{t}, b, t) = t - u(a_{t}, b, t)$$

$$= t - \left[v(a_{t}, t) - (t - b) \cdot \frac{d}{dt}(t - g(a_{t}, b, t))\right]$$

$$= t - v(a_{t}, t) + (t - b) \cdot \left(1 - \frac{d}{dt}g(a_{t}, b, t)\right)$$

$$= 2t - b - v(a_{t}, t) - (t - b) \cdot \frac{d}{dt}g(a_{t}, b, t)$$
(55)

Using the total derivative from Equation 49, substitute into the residual reformulation and group terms:

$$g_{\text{tot}} = 2t - b - v(a_t, t) - (t - b) \cdot \text{jvp}$$
 (56)

Inference: When b = 0, t = 1, the final action is recovered as:

$$a = e - u(e, 0, 1) = e - (1 - g(e, 0, 1))$$
(57)

²For brevity, we omit variants $g(a_t, b, t) = e - u_\theta(a_t, b, t)$, as it has already been discussed in the preceding section.

Variant 4: $\phi = 2a_t \Rightarrow g = 2a_t - u_\theta(a_t, b, t)$ Substituting *MeanFlow Identity* equation into the residual function:

$$g(a_{t}, b, t) = 2a_{t} - u(2a_{t}, b, t)$$

$$= 2a_{t} - \left[v(a_{t}, t) - (t - b) \cdot \frac{d}{dt}(2a_{t} - g(a_{t}, b, t))\right]$$

$$= 2a_{t} - v(a_{t}, t) + (t - b) \cdot \left(2 \cdot \frac{da_{t}}{dt} - \frac{d}{dt}g(a_{t}, b, t)\right)$$
(58)

Recall that $\frac{da_t}{dt} = v(a_t, t)$. Then we have:

$$g(a_t, b, t) = 2a_t - v(a_t, t) + 2(t - b)v(a_t, t) - (t - b) \cdot \frac{d}{dt}g(a_t, b, t)$$

$$= 2a_t + (2t - 2b - 1)v(a_t, t) - (t - b) \cdot \frac{d}{dt}g(a_t, b, t)$$
(59)

By applying the total derivative from Equation 49 and substituting it into the residual formulation, we simplify the expression to obtain:

$$g_{\text{tgt}} = 2a_t + (2t - 2b - 1)v(a_t, t) - (t - b) \cdot \text{jvp}$$
(60)

Inference: When b = 0, t = 1, we have:

$$a = e - u(e, 0, 1) = e - [2a_t - g(a_t, 0, 1)] = g(e, 0, 1) - e$$

$$(61)$$

Consequently, our theoretical framework offers a principled explanation for the failure of certain residual formulations, such as $g_{\theta} = e - u_{\theta}$ and $g_{\theta} = et - u_{\theta}$, to serve as effective reformulations of u_{θ} . Specifically, these variants choose $\phi(e,b,t) = e$ or et, which are neither continuous nor analytic with respect to the input variables (a_t,b,t) , and fail to depend functionally on the conditioning trajectory. As a result, the decomposition becomes ill-posed: the network u_{θ} is forced to approximate an unstructured and potentially discontinuous residual, thereby violating the assumptions required for universal approximation and stable optimization.

This theoretical insight is directly supported by empirical results on toy datasets, as detailed in Table 3. Variants that violate our proposed sufficient conditions—such as $g_{\theta} = e - u_{\theta}$ and $g_{\theta} = e t - u_{\theta}$ —consistently exhibit degraded performance. Specifically, these settings lead to mode collapse, poor convergence, and substantial distributional shift, as reflected by high 2-Wasserstein distances ($W_2 = 0.591$ and 0.393, respectively) and visibly distorted output distributions.

In contrast, all residual formulations that satisfy our theoretical conditions—such as $a_t - u_\theta$, $2a_t - u_\theta$, $t - u_\theta$, and even the constant form $2 - u_\theta$ —demonstrate stable training dynamics and successfully recover the target distribution. These formulations achieve low Wasserstein distances (all near 0.263) and generate samples that are visually indistinguishable from those produced by the original MeanFlow. The alignment between the "Theory-Compatible" column in Table 3, the numerical metric, and the distribution visualizations provides strong empirical validation of our theoretical framework. Notably, this holds even for seemingly simple choices of ϕ , such as constant or linear functions of time and input, as long as they remain fixed, analytic, and input-dependent. Subsequently, we examined whether each formulation permits direct noise-to-action mapping via the network, and ultimately selected the residual form $a_t - u_\theta$ as shown in Table 3. This choice is motivated by the fact that it is the only variant that simultaneously satisfies our theoretical conditions and enables direct generation of actions from noise through the network. Additionally, we evaluate the practical effectiveness of our reformulation using the same multimodal toy example shown in Fig. 9. Under the same number of training epochs, our approach consistently outperforms distillation-based generative baselines, demonstrating a superior capacity to capture complex multimodal action distributions.

Summary. The residual formulation

$$g_{\theta}(a_t, b, t) = a_t - u_{\theta}(x_t, b, t) \tag{62}$$

provides a theoretically grounded parameterization for controllable noise-to-action mappings, while retaining the full expressivity of the original MeanFlow. It is worth noting that this residual form constitutes only one valid instantiation within our general framework; any formulation employing a fixed, continuous, analytic function ϕ , independent of u_{θ} , equally satisfies the sufficient conditions for expressivity and stability.

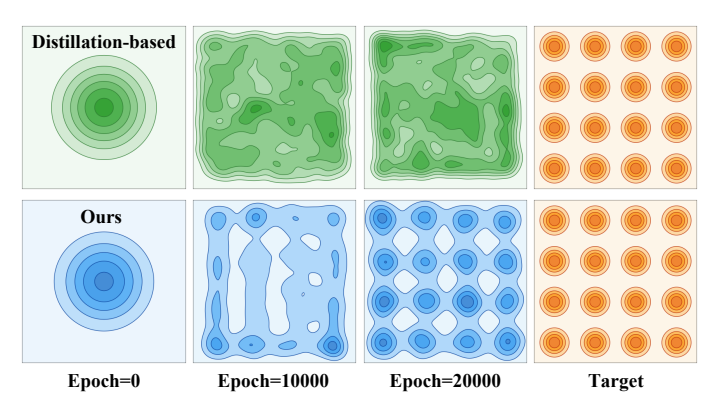


Figure 9: Toy example comparing the multimodal representation learning capabilities of the distillation-based one-step flow matching method and our proposed one-step policy model. The proposed model demonstrates improved accuracy and efficiency in capturing distinct modes of the target distribution, highlighting its superior ability to represent complex multimodal structures.

Table 3: Comparison of Reformulation Variants. Each row shows a formulation of g, its regression target, inference procedure, theoretical properties, and toy experiment performance. The reported metric is the 2-Wasserstein distance, which quantifies distribution-level alignment between generated actions and ground-truth samples in a 2D toy task. Theory-Compatible? indicates whether the reformulation variants g conforms to our theoretical framework. Noise-to-Action? indicates whether the method supports direct generation of actions from noise via a single forward pass.

g	Target	Inference	Theory- Compatible?	Noise-to- Action?	Metrics (↓)	Performance on Toy Experiment
u	$v-(t-b)\cdot \mathtt{jvp}$	g(e,0,1)	✓	X	0.263	
$a_t - u$	$a + (t - b)v - (t - b) \cdot jvp$	g(e,0,1)	1	1	0.262	
e-u	$e-v-(t-b)\cdot \mathtt{jvp}$	g(e,0,1)	х	✓	0.591	
et-u	$\begin{array}{c} (2t-b)e-v-(t-\\ b)\cdot \mathtt{j}\mathtt{v}\mathtt{p} \end{array}$	g(e,0,1)	х	✓	0.393	
2-u	$2-v-(t-b)\cdot \mathtt{jvp}$	e - (2 - g(e, 0, 1))	1	×	0.267	
t-u	$2t-b-v-(t-b)\cdot \mathtt{jvp}$	e - (1 - g(e, 0, 1))	1	×	0.264	
$2a_t - u$	$2a_t + (2t - 2b - 1) \cdot \\ v - (t - b) \cdot jvp$	g(e,0,1)-e	/	×	0.263	

¹ ✓ indicates "Yes"; X indicates "No".

² Metric denotes the 2-Wasserstein distance (W_2) , which quantifies the transport cost between predicted and ground-truth action distributions, offering a smooth and geometry-aware measure of distributional discrepancy. ³ jvp denotes jvp $(g, (a_t, b, t), (v, 0, 1))$ for simplicity. ⁴ $e \sim \mathcal{N}(0, I_d)$, $a_t = (1 - t)a + te$, and v = e - a.

Table 4: Full offline RL results. We present the full results on the 73 OGBench and D4RL tasks. (*) indicates the default task in each environment. The results are averaged over 8 seeds (4 seeds for pixel-based tasks) unless otherwise mentioned.

Tame the proving a reingle table taken 1 or 1 o		Gaus	ssian Po	licies	Diffu	sion Pol	licies		Fl	ow Polic	ies	
Section	Task	BC	IQL	ReBRAC	IDQL	SRPO	CAC	FAWAC	FBRAC	IFQL	FQL	Ours
Section		0 ±0					42 ± 7					
Section Sect												
Statistics												
Section	antmaze-large-navigate-singletask-task5-v0	10 ±3	54 ± 22	90 ±2	$2_{\pm 2}$	1 ±1	55 ± 6	9 ±5	76 ± 8	38 ±18	83 ±4	87 ±2
Description												
	antmaze-giant-navigate-singletask-task5-v0	1 ±1	19 ±7		0 ±1	0 ±0	0 ±0	0 ±0		13 ±9	16 ±28	0 ±0
Numanoidanear-endulm-navigate-singletank-tack+v0 (*) 0.5 0.5 1.5 1.5 1.5 0.5												
		_										
Introcer-race-nary gate-eingletask-taski-v0 2	humanoidmaze-large-navigate-singletask-task4-v0								0 ±0			
### Annable Control of Part Annable Contro												
International content and a												
matroscor-rarean-navigate-singletank-tank+v0 (*)												$60{\scriptstyle~\pm4}$
Cube-single-play-singletack-tack-tack-to(+)	antsoccer-arena-navigate-singletask-task4-v0 (*)		3 ± 2									43 ± 2
cube-single-play-singletack-tankX-v0 (*) 3 ± 1 st 5 ± s 9 ± s												
cube-single-play-singletask-task4-vo 9 ab 3												
cube-double-play-singletak-taski-vo 8 ab 27 b 87 b 89 b 80 b 78 b 70 as 77 ar 93 as 95 ab cube-double-play-singletak-taski-vo 0 ab 1 ab 1 ab 1 ab 1 ab 1 ab 1 ab 2												
Cube-double-play-singletask-task1-v0												
cube-double-play=singletask-task2+00 (*) 0.80 1 st. 7 ss. 1 [0 st. 0 0 st. 0 2 st. 2 st. 22												
cube-double-play=singletask-task4-v0 0 aboole of the second play singletask-task4-v0 0 aboole of the sec												
Scene-play-singletask-task-v0	cube-double-play-singletask-task3-v0			4 ± 1							$22{\scriptstyle~\pm5}$	2 ± 1
Scene-play-singletask-task1-v0												
Scene-play-singletask-task-v0 (*)												
Scene-play-singletask-task4-v0 2 ± 2 0 ± 1 32 ± 7 55 ± 10 0 ± 0 ± 0 ± 0 0 ± 0 0 ± 0 0 ± 0 0 ± 0 0 ± 0 0 ± 0 0 ± 0 0 ± 0 0 ± 0 0 ± 0 ± 0 0 ± 0 0 ± 0 0 ± 0 0 ± 0 0 ± 0 0 ± 0 0 ± 0 0 ± 0 0 ± 0 0 ± 0												
Scene-play-singletask-taski-v0		$1_{\pm 1}$	32 ± 7	55 ± 16	$94_{\pm4}$	4 ± 4	$49_{\ \pm 16}$	38 ± 9	78 ± 14	$54_{\pm 19}$	$98_{~\pm1}$	98 ± 1
Puzzle-3x3-play-singletask-task1-v0												
puzzle-3x3-play-singletask-task3-v0												
Digital of Start Paragraph Start												
Puzzle-3x3-play-singletask-task1-v0	puzzle-3x3-play-singletask-task3-v0											
Duzzle-4x4-play-singletask-taskl-v0												
$\begin{array}{c ccccccccccccccccccccccccccccccccccc$												
$\begin{array}{c ccccccccccccccccccccccccccccccccccc$									5 ± 3			
$\begin{array}{c ccccccccccccccccccccccccccccccccccc$												
antmaze-umaze-v2 antmaze-umaze-diverse-v2 47 54 84 80 82 66 ±1; 55 ±7 82 ±0 62 ±12 89 ±1 79 ±2 antmaze-medium-play-v2 0 66 90 84 81 49 ±0 52 ±12 77 ±7 56 ±15 78 ±7 86 ±2 antmaze-medium-diverse-v2 1 74 84 85 75 0 ±1 44 ±15 77 ±6 60 ±25 71 ±13 78 ±2 antmaze-large-play-v2 0 42 52 64 54 0 ±0 10 ±6 32 ±1 55 ±9 84 ±7 80 ±3 antmaze-large-play-v2 0 30 64 68 54 0 ±0 10 ±6 32 ±1 55 ±9 84 ±7 80 ±3 antmaze-large-diverse-v2 0 30 64 68 54 0 ±0 10 ±6 32 ±1 55 ±9 84 ±7 80 ±3 antmaze-large-diverse-v2 0 30 64 68 54 0 ±0 10 ±6 32 ±1 55 ±9 84 ±7 80 ±3 antmaze-large-diverse-v2 0 30 64 68 54 0 ±0 10 ±6 32 ±1 55 ±9 84 ±7 80 ±3 antmaze-large-diverse-v2 0 30 64 68 54 0 ±0 10 ±6 32 ±1 55 ±9 84 ±7 80 ±3 antmaze-large-diverse-v2 0 30 64 58 54 0 ±0 10 ±6 32 ±1 55 ±9 84 ±7 80 ±3 antmaze-large-diverse-v2 0 30 64 58 54 0 ±0 10 ±6 32 ±1 55 ±9 84 ±7 80 ±3 antmaze-large-diverse-v2 0 30 64 ±7 65 ±1 65 ±7 65 ±0 67 ±0 80 ±11 74 ±1 53 ±6 84 ±7 9en-cloned-v1 10 128 152 140 ±6 134 ±4 103 ±9 118 ±6 119 ±7 139 ±5 142 ±6 135 ±3 door-human-v1 2 3 0 6 ±2 3 ±3 5 ±2 2 ±1 4 ±2 7 ±2 0 ±0 1 ±1 door-expert-v1 105 107 106 105 ±1 105 ±0 98 ±3 103 ±1 104 ±1 104 ±2 104 ±1 104 ±1 hammer-cloned-v1 1 2 5 2 ±1 1 ±1 2 ±0 2 ±1 2 ±1 3 ±1 11 ±0 ±0 1 ±0 ±1 2 ±1 11 ±1 10 ±1 1												
$\begin{array}{c ccccccccccccccccccccccccccccccccccc$												
$\begin{array}{c ccccccccccccccccccccccccccccccccccc$	antmaze-umaze-diverse-v2	47	54	84	80	82	66 ± 11	55 ± 7	82 ± 9	62 ± 12	$89{\scriptstyle~\pm5}$	$79_{\pm 2}$
$\begin{array}{c ccccccccccccccccccccccccccccccccccc$												
$\begin{array}{ c c c c c c c c c c c c c c c c c c c$												
$\begin{array}{c ccccccccccccccccccccccccccccccccccc$		0	30	64	68	54	0 ±0	16 ± 10	20 ± 17	64 ± 8	$83_{~\pm4}$	76 ± 1
$\begin{array}{c ccccccccccccccccccccccccccccccccccc$	•											
$ \begin{array}{c ccccccccccccccccccccccccccccccccccc$												
$\begin{array}{c ccccccccccccccccccccccccccccccccccc$	_ -	2	3							7 ± 2		
$\begin{array}{c ccccccccccccccccccccccccccccccccccc$												
$\begin{array}{c ccccccccccccccccccccccccccccccccccc$												
$ \begin{array}{c ccccccccccccccccccccccccccccccccccc$	hammer-cloned-v1	1	2	5	$2{\scriptstyle~\pm 1}$	2 ± 1	$1_{\pm 1}$	1 ± 0	2 $_{\pm 1}$	$2_{\pm 1}$	11 ± 9	$10{\scriptstyle~\pm5}$
$ \begin{array}{c ccccccccccccccccccccccccccccccccccc$												
$ \begin{array}{c ccccccccccccccccccccccccccccccccccc$												
$\begin{array}{cccccccccccccccccccccccccccccccccccc$												
$\begin{array}{cccccccccccccccccccccccccccccccccccc$		-			_	_	_	-				
visual-puzzle-3x3-play-singletask-task1-v0 (1) $$		_				_	_	_				
		_			_	_	_	_				
		_			_	_	_	_				

C. Additional Results

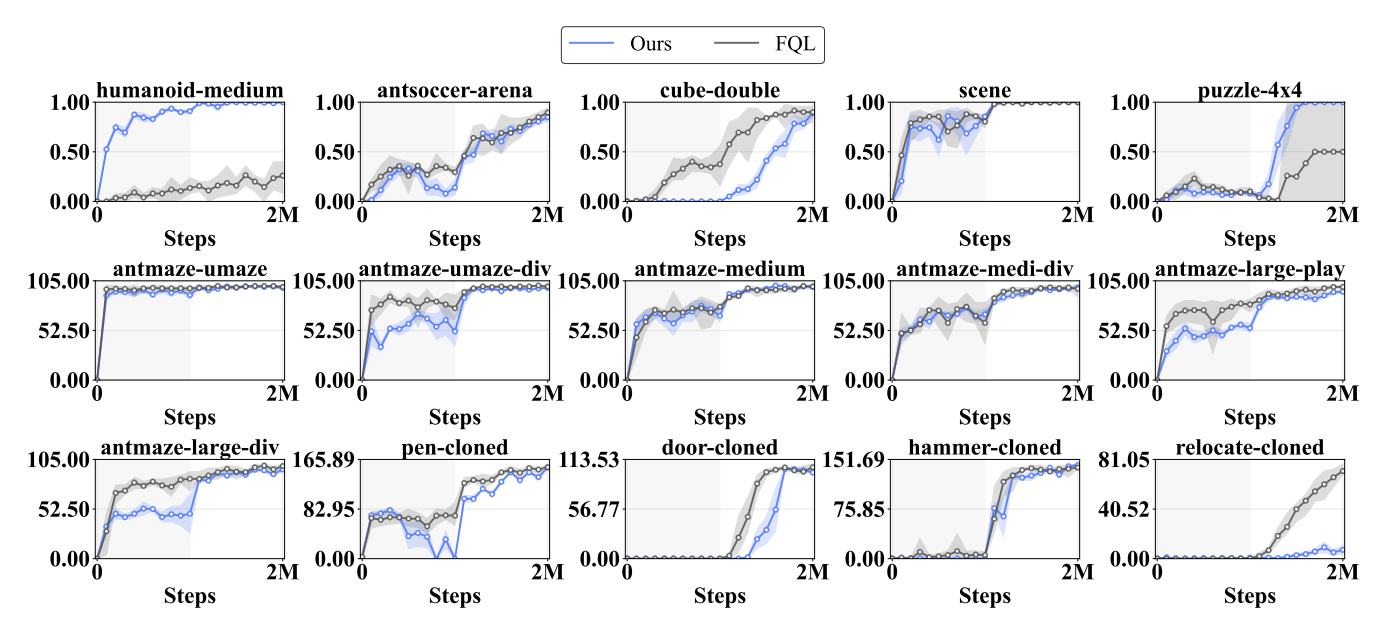


Figure 10: Offline-to-online RL results. Online fine-tuning starts at 1M steps. The results are averaged over 8 seeds unless otherwise mentioned.

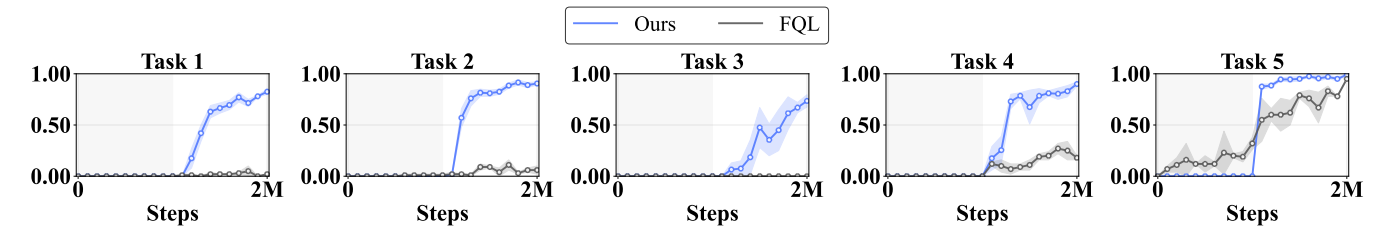


Figure 11: Offline-to-online RL results on antmaze-giant-navigate-singletask. Although our method starts from suboptimal offline performance, it exhibits rapid adaptation and consistently surpasses FQL across all challenging tasks during the online fine-tuning phase, demonstrating strong online learning capability.

D Implementation Details.

Critic network architectures. Following FQL (Park, Li, and Levine 2025), we employ [512, 512, 512, 512]-sized multi-layer perceptrons (MLPs) for critic function networks. To improve training stability, we also apply layer normalization to the value networks.

Actor Network architectures. Since our method heavily relies on accurate modeling of the time variable, particularly in the context of Jacobian-vector product (JVP) computations, we choose DiT as the underlying network architecture. We use a shallow Transformer-based policy adapted from DiT (Peebles and Xie 2023), with 3 layers, 2 attention heads, and a hidden size of 256. A feature embedding maps 1D observation-action inputs, and the network includes time and positional embeddings, residual mixing (scale 0.1). Specifically, we apply gradient clipping (norm 1.0) and zero-initialised final projection for stability.

Image processing. For pixel-based environments, we adopt a lightweight variant of the IMPALA encoder and apply random-shift augmentation with a probability of 0.5, following the official OGBench implementation (Park et al. 2025).

Training and evaluation. We train all networks for 1M gradient steps on state-based OGBench tasks, and for 500K steps on both D4RL and pixel-based OGBench tasks. Evaluation is performed every 100K steps using 50 rollout episodes.

For OGBench, we follow the official evaluation protocol (Park et al. 2025), reporting the average success rate across the final three evaluation epochs: 800K, 900K, and 1M for state-based tasks; 300K, 400K, and 500K for pixel-based tasks.

For D4RL, we report the performance at the final training step. In offline-to-online RL experiments (2), we report results at both 1M and 2M gradient steps.

Loss Metrics To define the regression loss for the target function g_{θ} , we adopt a powered ℓ_2 loss of the form:

$$\mathcal{L}_{\gamma} = \|\Delta\|_2^{2\gamma}, \quad \text{where} \quad \Delta = g_{\theta} - g_{\text{tgt}}, \ \gamma > 0.$$
 (63)

Following (Song and Prafulla 2024; Geng et al. 2025), its gradient can be written as:

$$\frac{d}{d\theta} \mathcal{L}_{\gamma} = \gamma \left(\|\Delta\|_{2}^{2} \right)^{\gamma - 1} \cdot \frac{d}{d\theta} \|\Delta\|_{2}^{2},\tag{64}$$

which corresponds to an adaptively weighted squared ℓ_2 loss. We adopt the following stabilised weight formulation:

$$w = \frac{1}{(\|\Delta\|_2^2 + c)^p}, \text{ where } p = 1 - \gamma, c > 0,$$
 (65)

and define the final loss as:

$$\mathcal{L}_{\text{final}} = \text{sg}(w) \cdot \|\Delta\|_2^2. \tag{66}$$

where $sg(\cdot)$ denotes the stop-gradient operator to prevent gradients from flowing through the adaptive weight. As shown in MeanFlow (Geng et al. 2025), the parameter p plays a significant role in determining the final performance. In our experiments, we conduct a preliminary study on the sensitivity of p and observe that setting p=0.2 consistently yields strong performance across tasks. We therefore recommend tuning this parameter when applying our method, as it can have a notable impact on both stability and accuracy.

Sampling time steps (b, t) Time steps play a critical role in the training of MeanFlow (Geng et al. 2025), as they are directly involved in the Jacobian–vector product (JVP) computation required for learning the flow dynamics. Same to original MeanFlow (Vaswani et al. 2017; Geng et al. 2025), we use positional embedding to encode the time variables, which are then combined and provided as the conditioning of the neural network.

However, we observed in our experiments that directly adopting the time step formulation from MeanFlow leads to training collapse. One possible reason is the significant difference in dimensionality between reinforcement learning and image generation: while the action space in RL typically has a low dimensionality (e.g., 5 to 21), image data often resides in much higher-dimensional spaces (e.g., at least $3 \times 32 \times 32$). This discrepancy causes uniform sampling of $(b,t) \sim \mathcal{U}(0,1)$ to introduce excessive randomness and instability during training.

To address this issue, we find that appropriately simplifying the original MeanFlow formulation—such as by setting b=0—can substantially reduce training complexity and make it feasible to learn effectively in low-dimensional action spaces. Accordingly, we explore both uniformly sampled discrete and continuous time steps from $\mathcal{U}(0,1)$ s, and conduct the experiments summarized in Table 5 to evaluate their impact. Our empirical observations suggest that this choice is highly sensitive to the underlying task complexity. As a result, we consider it as a task-dependent hyperparameter subject to tuning. In particular, the choice of the time step should be adapted to the task complexity and the amount of available data. We recommend trying the following settings in order of expressiveness and stability: (i) both b and t as continuous variables, (ii) fixing b=0 while keeping t continuous, and (iii) finally, using discrete timestamps for t with b=0. This progressive relaxation enables practitioners to balance modeling flexibility and computational efficiency.

Table 5: Performance under different time step configurations: discrete 50 steps, discrete 100 steps, and continuous sampling.

	Time Step Strategy						
Environment	Disc.(50)	Disc.(100)	Cont.				
antmaze-large-task1	91 ± 2	78 ±6	49 ± 10				
humanoidmaze-large-task1	53 ± 5	$44~\pm 5$	42 ± 2				
cube-single-task4	88 ± 2	89 ± 3	95 ± 2				
antmaze-umaze-v2	96 ± 1	95 ± 1	98 ± 1				
antmaze-medium-diverse	78 ± 2	78 ± 4	73 ± 5				
pen-human-v1	80 ± 5	84 ± 7	$72{\scriptstyle~\pm1}$				

BC coefficient α . The BC coefficient α is the key hyperparameter in our method, as it directly controls the trade-off between behavior cloning and value-based learning. We begin with a coarse grid search over 1, 10, 100, 1000, 1000 across all tasks. Based on the preliminary results, we identify a promising subrange and perform a finer-grained search within that interval for each environment. The optimal value of α varies significantly across tasks and must be carefully tuned to achieve strong performance. Given its sensitivity and importance, we consider the automatic adaptation of α an important direction for future work. In particular, we plan to explore multi-objective optimisation techniques that jointly balance imitation fidelity and reward maximisation, thereby reducing the reliance on exhaustive manual tuning.

Baselines. We adopt the same baseline configurations as those used in Flow Q-Learning (FQL) (Park, Li, and Levine 2025), ensuring full alignment in implementation and evaluation protocols. All baselines are implemented using the official FQL codebase without modification, and hyperparameters are retained as reported in (Park, Li, and Levine 2025).

E Experimental Details

E.1 Environments and Datasets

OGBench (Park et al. 2025). OGBench serves as our primary benchmark. We adopt a total of 10 state-based and 5 pixel-based tasks drawn from OGBench, comprising 50 state-based and 5 pixel-based offline RL tasks. Originally designed for offline goal-conditioned reinforcement learning, we utilise the single-task variants (denoted as "-single-task") of OGBench to benchmark conventional reward-maximising offline RL algorithms.

Each OGBench environment offers five distinct evaluation goals, corresponding to tasks named <code>-singletask-task1</code> through <code>-singletask-task5</code>, with one designated as the default task (denoted simply as <code>-singletask</code>). For a given evaluation goal, the corresponding single-task dataset provides transitions labelled with a semi-sparse reward function. This reward is computed as the negative number of remaining subtasks in a given state.

In locomotion environments, each task contains a single subgoal (e.g., "reach the target"), yielding rewards of either -1 or 0. In contrast, manipulation environments typically involve multiple subtasks (e.g., "open the drawer", "turn the button blue"), and the reward ranges from $-n_{\rm task}$ to 0, where $n_{\rm task}$ denotes the number of subtasks, up to 16 in our selected environments. Episodes terminate upon successful completion of the specified goal.

We use the following datasets in our experiments, each providing five tasks:

• State-based datasets:

- antmaze-large-navigate-v0
- antmaze-giant-navigate-v0
- humanoidmaze-medium-navigate-v0
- humanoidmaze-large-navigate-v0
- antsoccer-arena-navigate-v0
- cube-single-play-v0
- cube-double-play-v0
- scene-play-v0
- puzzle-3x3-play-v0
- puzzle-4x4-play-v0

· Pixel-based datasets:

- visual-cube-single-play-v0
- visual-cube-double-play-v0
- visual-scene-play-v0
- visual-puzzle-3x3-play-v0
- visual-puzzle-4x4-play-v0

These environments present diverse challenges. The antmaze and humanoidmaze tasks require controlling quadrupedal (8-DOF) or humanoid (21-DOF) agents to reach target positions in maze layouts. antsoccer requires navigating a quadrupedal agent while dribbling a ball to a specified location. Manipulation tasks such as cube, scene, and puzzle involve robot arms interacting with various objects. In particular, scene tasks entail long-horizon control of multiple objects (up to 8 subtasks), while puzzle tasks demand combinatorial generalisation.

Pixel-based tasks (prefixed with visual-) involve controlling agents solely from raw pixel observations of size $64 \times 64 \times 3$. We employ standard task types: navigate for locomotion and play for manipulation. These datasets are highly suboptimal, comprising trajectories collected during the execution of *random* tasks (e.g., reaching random goals or manipulating random objects), thus necessitating strong trajectory stitching capabilities. For state-based environments, we evaluate all five tasks, whereas for pixel-based environments, only singletask-task1 is used due to computational constraints.

Evaluation follows the original benchmark protocol, using binary task success rates (in percentage).

D4RL (Fu et al. 2020). To facilitate direct comparison with prior work, we additionally evaluate on 18 challenging tasks from the D4RL benchmark. These include six antmaze tasks and twelve adroit tasks:

- $\bullet \ \, antmaze-umaze-v2, antmaze-umaze-diverse-v2, antmaze-medium-play-v2, antmaze-medium-diverse-v2, antmaze-large-play-v2, antmaze-large-diverse-v2, antmaze-large-diverse-dive$
- pen-human-v1, pen-cloned-v1, pen-expert-v1
- door-human-v1, door-cloned-v1, door-expert-v1
- hammer-human-v1, hammer-cloned-v1, hammer-expert-v1
- relocate-human-v1, relocate-cloned-v1, relocate-expert-v1

The D4RL antmaze tasks share a similar objective with those in OGBench but use different (and typically less challenging) maze configurations, datasets, and evaluation goals. The adroit suite (pen, door, hammer, and relocate) involves high-dimensional (24-DOF) dexterous manipulation tasks. Evaluation metrics follow the original D4RL protocol: binary task success rates for antmaze and normalised returns for adroit.

To prevent excessively large numerical ranges in the input observations, we apply *feature-wise normalisation* to the dataset. This preprocessing step ensures that the input distributions are well-conditioned, which is beneficial for stable and efficient Transformer training.

E.2 Hyper-parameters Our hyperparameter configuration is organized into two main categories. The first encompasses general-purpose settings that are held constant across all tasks, including network architecture, optimisation details, and regularization coefficients (see Table 6). The second category includes task-specific parameters—such as the behavior cloning coefficient α , the number of action candidates, and time_steps—which are individually tuned for each environment to ensure stable training dynamics and optimal performance (see Table 7).

Table 6: Hyperparameters in Experiments

Parameter	Value	Description
	General Se	
sigma	1.0	Standard deviation of injected noise
batch_size	256	Number of samples per batch
q_agg	mean	Target Q aggregation method
normalize_q_loss	False	Normalize Q loss term
noise_type	gaussian	Noise distribution type
optimizer	Adam (Adam et al. 2014)	Optimizer of networks
gradient steps	1000000 (default), 500000	Total gradient updates
discount γ	0.99 (default), 0.995	Keep same as FQL(Park, Li, and Levine 2025)
image aug. prob.	0.5	Probability of image augmentation
	Critic Net	work
value_hidden_dims	(512, 512, 512, 512)	Hidden layer sizes
layer_norm	True	Apply layer normalization
lr	1e-4	Learning rate
lr_schedule	constant	Learning rate schedule
gradient clipping	1.0	Maximum gradient norm
network initialization	kaiming_init	Network initialization techniques
	Actor Net	work
lr	$1\mathrm{e}{-4}$	Learning rate
lr_schedule	cosine_with_warmup	Learning rate schedule
lr_min_ratio	0.1	Minimum ratio in cosine scheduler
actor_hidden_dims	256	Hidden size of actor MLP
actor_depth	3	Number of transformer layers
actor_num_heads	2	Number of attention heads
actor_layer_norm	False	Use layer norm in actor
discount	0.99	Discount factor γ
tau	0.005	Target network update rate
alpha	Task-dependent	See Table 7
tanh_squash	False	Use tanh at actor output
use_output_layernorm	False	Norm at final actor output
gradient clipping	1.0	Maximum gradient norm
network initialization	zero_init	Network initialization techniques
	Flow-related	
adaptive_gamma	0.8	Velocity loss weight
adaptive_c	$1\mathrm{e}{-4}$	Position loss weight
bound_loss_weight	1.0	Weight for boundary loss
time_steps	Task-dependent	See Table 7
	Best-of-N Sa	
num_candidates	Task-dependent	See Table 7
action_mode	best	Action selection strategy
	Alpha Sche	8
use_dynamic_alpha	True	Enable dynamic α tuning
alpha_update_interval	2000	Adjustment frequency
loss_multiplier_threshold	5	Threshold to increase α
alpha_increase_factor	1.2	Multiplier for increase
alpha_decrease_factor	0.8	Multiplier for decrease
loss_history_window_size	20	History window size

Table 7: Task-Specific Hyperparameter Settings. We present the hyperparameters (α , number of candidates, and time steps) for all tasks. (*) indicates the default task in each environment.

Environment	alpha	num_candidates	time_steps
antmaze-large-navigate-singletask-task1-v0 (*)	10	5	50
antmaze-large-navigate-singletask-task2-v0	1000	5	50
antmaze-large-navigate-singletask-task3-v0	2350	5	50
antmaze-large-navigate-singletask-task4-v0	7	1	50
antmaze-large-navigate-singletask-task5-v0	15	5	50
antmaze-giant-navigate-singletask-task1-v0 (*)	1000	1	50
antmaze-giant-navigate-singletask-task2-v0	1000	1	50
antmaze-giant-navigate-singletask-task3-v0	1000	1	50
antmaze-giant-navigate-singletask-task4-v0	1000	1	50
antmaze-giant-navigate-singletask-task5-v0	1000	1	50
humanoidmaze-medium-navigate-singletask-task1-v0 (*)	150	5	50
humanoidmaze-medium-navigate-singletask-task2-v0	10000	5	100
humanoidmaze-medium-navigate-singletask-task3-v0	9400	1	100
humanoidmaze-medium-navigate-singletask-task4-v0	60	1	50
humanoidmaze-medium-navigate-singletask-task5-v0	150	5	50
humanoidmaze-large-navigate-singletask-task1-v0 (*)	10000	5	50
humanoidmaze-large-navigate-singletask-task2-v0	1000	5	50
humanoidmaze-large-navigate-singletask-task3-v0	1000	5	100
humanoidmaze-large-navigate-singletask-task4-v0	1000	1	50
humanoidmaze-large-navigate-singletask-task5-v0	10000	5	10000
antsoccer-arena-navigate-singletask-task1-v0	200	10	50
antsoccer-arena-navigate-singletask-task2-v0	100	5	100
antsoccer-arena-navigate-singletask-task3-v0	1100	5	50
antsoccer-arena-navigate-singletask-task4-v0 (*)	10000	5	50
antsoccer-arena-navigate-singletask-task5-v0	200	5	50
<u>-</u>	200	5	50
cube-single-play-singletask-task1-v0 cube-single-play-singletask-task2-v0 (*)	200	5 1	50 50
cube-single-play-singletask-task3-v0	50	1	100
cube-single-play-singletask-task4-v0	11000	5	10000
cube-single-play-singletask-task5-v0	180	1	50
	200	5	50
<pre>cube-double-play-singletask-task1-v0 cube-double-play-singletask-task2-v0 (*)</pre>	200 120	5 5	50 50
cube-double-play-singletask-task2-v0 (*) cube-double-play-singletask-task3-v0	180	5	50
	200	5	50
cube-double-play-singletask-task4-v0 cube-double-play-singletask-task5-v0	200 250	5 5	50 50
cube double play singletask tasks vo			
scene-play-singletask-task1-v0	8000	5	10000
scene-play-singletask-task2-v0 (*)	11000	5	50
scene-play-singletask-task3-v0	12000	5	50
scene-play-singletask-task4-v0	9800	1	10000
scene-play-singletask-task5-v0	8000	5	50
puzzle-3x3-play-singletask-task1-v0	1000	5	100
puzzle-3x3-play-singletask-task2-v0	30	1	50
puzzle-3x3-play-singletask-task3-v0	60	1	50
puzzle-3x3-play-singletask-task4-v0 (*)	100	5	50
puzzle-3x3-play-singletask-task5-v0	60	1	50
puzzle-4x4-play-singletask-task1-v0	1000	5	100
puzzle-4x4-play-singletask-task2-v0	5550	5	100
puzzle-4x4-play-singletask-task3-v0	1200	5	100
puzzle-4x4-play-singletask-task4-v0 (*)	8000	5	10000
puzzle-4x4-play-singletask-task5-v0	2450	5	50
antmaze-umaze-v2	100	5	10000
antmaze-umaze-diverse-v2	130	5	100
antmaze-medium-play-v2	10	5	50
antmaze-medium-diverse-v2	50	5	50
antmaze-large-play-v2	10	5	100
antmaze-large-diverse-v2	6	5	50
pen-human-v1	10000	5	100
pen-cloned-v1	10000	5	100
pen-expert-v1	10000	5	50
door-human-v1	5000	1	100
door-cloned-v1	9000	5	50
door-expert-v1	10000	5	50
hammer-human-v1	7000	1	100
nammer-numan-vi hammer-cloned-v1	11000	5	100
hammer-expert-v1	12000	5	50
nammer-expert-v1 relocate-human-v1	10000	5 5	100
		5 5	50
relocate-cloned-v1 relocate-expert-v1	10000 15000	5 5	50 100
-			
visual-cube-single-play-singletask-task1-v0	360	5	100
	350	5	100
	200		
visual-scene-play-singletask-task1-v0	300	1	100
visual-cube-double-play-singletask-task1-v0 visual-scene-play-singletask-task1-v0 visual-puzzle-3x3-play-singletask-task1-v0	300 300	1 5	100